Table 2
Cardiac physiological characteristics of control and morphant zebrafish embryos

	Control	Morphant	*P*
Dd (μm)	79.6 ± 3.7	117 ± 10.4	<0.0001
Ds (μm)	50.3 ± 6.5	76.0 ± 7.0	<0.0001
FS (%)	36.9 ± 7.1	34.9 ± 4.1	NS
HR (bpm)	184 ± 14.5	216 ± 24.7	0.0017

Values are mean ± SEM. n = 12 per group. HR, heart rate.

reassembly through MLC2v phosphorylation. Similar findings have previously been reported using recombinant constitutively active skMLCK (13). We further elucidated the physiologic roles of endogenous cardiac-MLCK using siRNAs. Decreases in MLC2v phosphorylation following the introduction of si-cMK significantly impaired epinephrine-induced sarcomere reassembly. Additionally, specific knockdown of cardiac-MLCK did not affect to the expression of other sarcomere-related proteins such as troponin T, desmin, and α-actinin. These proteins are thought to have important roles in sarcomere and myofibril formation (17–19). Thus, in cardiomyocytes, phosphorylation of MLC2v by cardiac-MLCK is an essential step for the initiation of sarcomere assembly. Upregulation of the protein levels of cardiac-MLCK in infantile rat heart supports this idea.

In this experimental model, no phenotypic alterations were observed following knockdown of cardiac-MLCK in cultured cardiomyocytes. This apparently paradoxical result occurred because phosphorylation of MLC2v is upregulated in cultured cardiomyocytes until 36 hours after plating, after which it is gradually downregulated. In the siRNA-mediated gene knockdown experiment, a reduction in the cardiac-MLCK protein level that was sufficient to decrease the phosphorylation of MLC2v was only obtained 60–72 hours after isolation. Therefore, by the time the required level of protein suppression was achieved, primary sarcomere assembly had been completed, and the subsequent decreases in MLC2v phosphorylation did not disrupt established sarcomere structures.

Reduction of cardiac-MLCK levels in zebrafish embryos through the injection of z-cMKaugMO resulted in ventral swelling, which has been previously reported to be a representative phenotype of cardiac abnormalities in zebrafish embryos (20, 21). The reliability of the results obtained with z-cMKaugMO was confirmed using multiple MOs that targeted not only cardiac-MLCK but also its substrate, MLC2v. In each experiment, reproducible results were obtained. Another MO that has 5-base mismatch to z-cMKaugMO was also examined as a negative control MO. Further analysis revealed dilatation of the ventricle with a thinned ventricular wall and immature sarcomeres in the morphants. The fragility of the ventricular wall as a result of insufficient sarcomere formation may have caused the ventricular dilatation. Although ventricular function as assessed by FS was preserved in the morphants, this might have been due to some positive inotropic effects, which were suggested by the increased heart rate observed in the z-cMKaugMO morphants. Although several reports have investigated the effects of MLC2v phosphorylation in striated muscle contractions, including in cardiac muscle, the in vivo ventricular role of MLC2v phosphory-

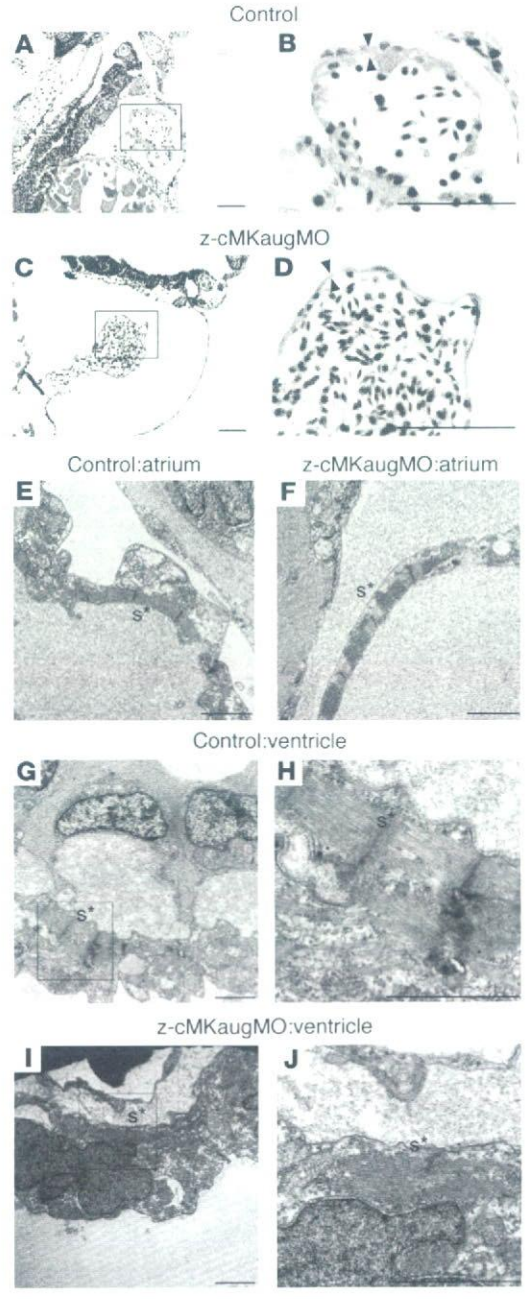

Figure 7
Histology of the zebrafish heart at 48 hpf. (**A**–**D**) Longitudinal sections stained with hematoxylin and eosin. Scale bars: 50 μm. (**E**–**J**) Transmission electron micrographs. Scale bars: 2 μm. (**A** and **B**) Histology of control zebrafish hearts at 48 hpf. A relatively thick ventricular wall was apparent (**B**, arrowheads). (**C** and **D**) Pericardial edema and a thinner ventricular wall (**D**, arrowheads) were observed in z-cMKaugMO morphants. (**E** and **F**) In the atria, the sarcomere structures were well differentiated in both the control embryos and the z-cMKaugMO morphants. In the ventricles of control embryos, robust sarcomere structures were observed (**G** and **H**), whereas the ventricles of the z-cMKaugMO morphants contained sparse and immature sarcomere structures (**I** and **J**). Images in **B**, **D**, **H**, and **J** show higher magnifications of the boxed areas in **A**, **C**, **G**, and **I**, respectively. Asterisks denote sarcomere structures (s).

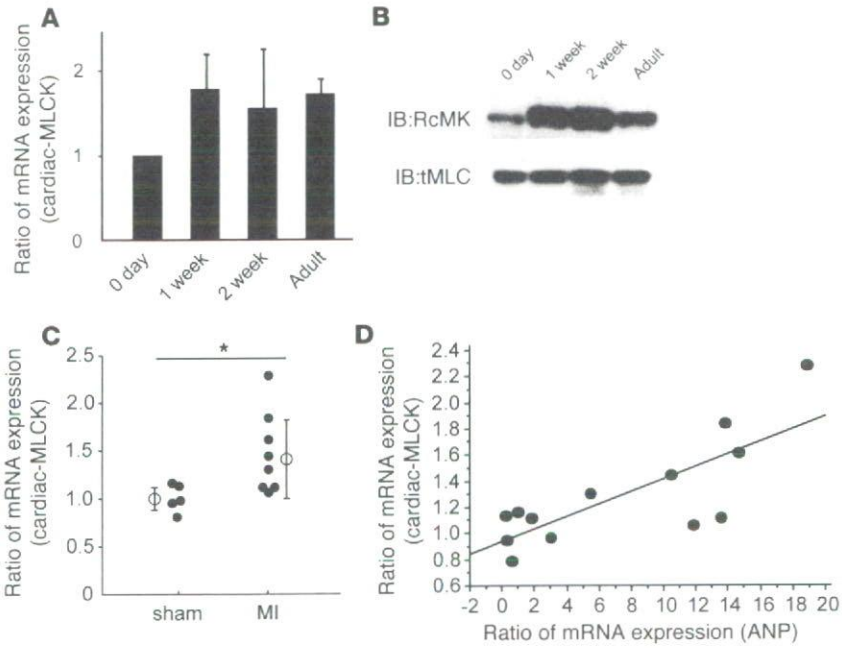

Figure 8
Expression of cardiac-MLCK is upregulated in infantile rat myocardia and failing rat myocardia. (**A**) mRNA expression of cardiac-MLCK was also upregulated in rat myocardia from 1 week after birth to adulthood. The levels of cardiac-MLCK protein were upregulated in infantile myocardia 1–2 weeks after birth. (**B**) The levels of cardiac-MLCK protein were upregulated in infantile myocardia 1–2 weeks after birth. (**C**) mRNA expression of cardiac-MLCK was significantly upregulated in failing rat myocardia. $n = 5$ (sham-operated); 8 (MI). Filled symbols represent values from individual mice; open symbols with bars represent mean ± SEM. $^*P < 0.05$. (**D**) The relative mRNA expression levels of ANP and cardiac-MLCK were significantly correlated ($r = 0.778$; $P < 0.005$).

lation is still not well understood (22, 23). To explore how cardiac-MLCK contributes to ventricular function, other experiments, such as a skinned fiber study, should be performed. A similar cardiac phenotype was reported in a recent study investigating the zebrafish *tel* mutant, in which the gene encoding MLC2v was disrupted by an *N*-ethyl-*N*-nitrosourea-induced mutation. The authors concluded that MLC2v is essential for the assembly of myosin thick filament (24). The observation of incomplete sarcomere formation resulting in a dilated ventricle in zebrafish embryos after injection of z-cMKaugMO can be explained by an inability to initiate sarcomere assembly as a result of reduced cardiac-MLCK levels.

Our results prompt the important question of how cardiac-MLCK is involved in the pathophysiology of CHF. In failing myocardia, decreases in myofibrillar proteins such as titin, myosin, and actin, together with the sarcomere defects, have been identified (25, 26). Reduced expression of MLC2v protein as a result of protease-mediated cleavage and reduced phosphorylation of MLC2v have also been reported in the myocardia of patients with dilated cardiomyopathy. These changes produced unstable, short myofilaments following defective assembly of the myosin thick filaments (27, 28). Our preliminary data also revealed that the protein expression of cardiac-MLCK and the extent of MLC2v phosphorylation were remarkably decreased in failing myocardia of trans-aortic constriction mice compared with those of sham-operated mice. Previous reports and our present results suggest that cardiac-MLCK may be upregulated to compensate for the lower expression and reduced phosphorylation of MLC2v. As a possible therapeutic modality in patients with CHF, upregulation of cardiac-MLCK may promote sarcomere reassembly and enhanced contractility of the failing heart.

Methods

Animals. All procedures were performed in conformity with the *Guide for the care and use of laboratory animals* (NIH publication no. 85-23, revised 1996) and were approved by the Osaka University Committee for Laboratory Animal Use.

Materials. We used commercially available anti-FLAG-M2 antibody and anti-FLAG-M2 affinity gel (Sigma-Aldrich), monoclonal mouse anti-troponin T cardiac isoform antibody (NeoMarkers), monoclonal mouse anti-human desmin Antibody (Dako Corp.), and polyclonal goat anti-α-actinin (N-19) antibody (Santa Cruz Biotechnology Inc.). Epinephrine hydrochloride was purchased from Sigma-Aldrich. We also generate RcMK, anti-human smMLCK, tMLC, and p-s15MLC.

Microarray analysis. For microarray analysis, 2 RNA samples of human normal myocardium and 12 samples of failing myocardium were used. Failing myocardium samples were obtained from severe CHF patients by Batista or Dor operation after obtaining the patients' written informed consent. PAP was measured 2–4 weeks before the operation, and ejection fraction (EF) was measured by echocardiography the day before the operation. Normal samples were purchased from Biochain Inc. Cardiac gene expression was determined using the HG-U95 Affymetrix GeneChip. All expression data were normalized by global scaling and analyzed by GeneSpring software (Agilent Technologies). All expression data were normalized per gene and analyzed after removing noise and unreliable data. PAP, EF, and BNP values were normalized to their median values, and the correlation between gene expression and the clinical parameters was evalu-

Table 3
Hemodynamic and echocardiographic characteristics of MI and sham-operated rats

	Sham	MI	*P*
LVSP (mmHg)	126.8 ± 10.9	125.5 ± 11.0	NS
HR (bpm)	415.4 ± 10.4	407.6 ± 23.0	NS
Max dP/dt (mmHg/s)	9,440 ± 644	5,845 ± 1,156	<0.01
LVEDP (mmHg)	3.2 ± 1.0	20.5 ± 8.2	<0.01
LVDd (mm)	6.8 ± 0.5	9.8 ± 0.3	<0.01
FS (%)	44.0 ± 7.8	12.0 ± 3.1	<0.01

Values are mean ± SEM. $n = 5$ (sham); 8 (MI). LVEDP, LV end-diastolic pressure; LVSP, LV systolic pressure; HR, heart rate; Max dP/dt, LV peak rate of change in pressure during isovolumic contraction.

ated. To further select genes that are expressed almost exclusively in heart, expression values for the candidate genes were retrieved in 24 major tissues for analysis from GeneExpress database (Gene Logic Inc.) containing GeneChip expression profiles of human samples.

RNA extraction, RT-PCR, and quantification. Rat tissues (20–50 mg) and zebrafish embryos at 72 hpf were homogenized in 1 ml RNA-Bee reagent (Tel-Test Inc.), and total RNA was isolated and converted to cDNA using Omniscript RT kit (QIAGEN) according to the manufacturer's instructions. Specific primers to amplify rat ANP, β myosin heavy chain, cardiac-MLCK, and GAPDH mRNA were purchased from Applied Biosystems. Quantitative RT-PCR reactions were run in duplicate using the ABI Prism 7700 Sequence Detector System (Applied Biosystems). The level of each transcript was quantified by the threshold cycle (Ct) method using GAPDH as an endogenous control. For RT-PCR, specific primers that cover the region of targeted exons were designed to amplify the transcripts of z-cardiac-MLCK and z-MLC2v. See Supplemental Methods for primer sequences.

Northern blot analysis. Commercially available human multiple tissue Northern blot and polyA$^+$ RNA of human heart and skeletal muscle were purchased from Clontech. Each polyA$^+$ RNA was reverse transcribed and amplified using an Omniscript RT kit (QIAGEN) according to the manufacturer's protocol. Hybridization probes of human cardiac-MLCK and smMLCK were amplified by PCR from cDNA of human heart, and a hybridization probe of human skMLCK was amplified by PCR from cDNA of human skeletal muscle. Membrane was hybridized to ^{32}P-labeled probe in Rapid-Hyb buffer (Amersham Bioscience) at 65°C for 1 hour. Final wash conditions were 0.1× SSC with 0.1% SDS at 65°C for 5 minutes. Hybridized membrane was visualized by autoradiography using the BAS system (Fuji).

Preparation and transfection of adenovirus constructs. Adenovirus constructs were generated using ViraPower Adenoviral Expression System (Invitrogen) essentially as instructed by the manufacturer. Adenovirus vectors encoding murine cardiac-MLCK and LacZ were infected to cultured cardiomyocytes for 12 hours in various MOIs. Protein collection and immunostaining were performed 48 hours after adenovirus infection.

Identification of the substrate of cardiac-MLCK. Recombinant cardiac-MLCK was expressed in HEK293T cells as FLAG-tagged protein. HEK293T cells expressing FLAG-tagged cardiac-MLCK were lysed with cell lysis buffer (20 mM MOPS, pH 7.0, 0.15 M NaCl, 10% glycerol, and 1% CHAPS) and recombinant cardiac-MLCK was purified by immunoprecipitation using anti-FLAG-M2 affinity gel (Sigma-Aldrich). Hearts dissected from male C57BL/6 mice (10–12 weeks of age) were mechanically homogenized using a Polytron homogenizer in 10 ml of tissue lysis buffer (30 mM MOPS, pH 6.8, 5% glycerol, 0.1% 2-mercaptoethanol, and 1 mM EGTA). Lysate was centrifuged for 40 minutes at 100,000 *g*, and 9 ml of supernatant was collected. Murine heart extracts were then applied to SP650 cation exchange column. The column was equilibrated with elution buffer A (30 mM MOPS, 5% glycerol, 0.1% 2-mercaptoethanol) at pH 6.8, and the extracts were eluted with a linear gradient of NaCl (0–0.5 M) at a flow rate of 1 ml/min. Each 1-ml fraction collected was incubated for 30 minutes with activated recombinant cardiac-MLCK, commercially available recombinant calmodulin (Upstate), 2 mM $CaCl_2$, and [γ-P^{32}]ATP and then subjected to SDS-PAGE. After drying, the gel was autoradiographed and visualized with BAS (Fuji). The fractions containing 20-kDa substrate (fractions 10 and 11) labeled with [γ-P^{32}]ATP were pooled and applied to a phenyl-RPLC column (5Ph-AR-300; nacalai tesque) equilibrated with 0.3% trifluoroacetic acid and 5% acetoritrile. Fractions were eluted with a linear gradient of 100% acetonitrile at flow rate of 1 ml/min. After separation with SDS-PAGE, the gel was simultaneously silver stained and autoradiographed. After identifying the 20-kDa substrate with silver-stained gel, the bands were excised from the gel, and proteins were identified by matrix-assisted laser desorption/ionization-time-of-flight mass spectrometry and peptide mass fingerprinting.

Preparation of cultured neonatal rat cardiomyocytes and gene silencing via RNA interference. Primary cultures of neonatal cardiomyocytes were prepared from Wistar rats as described previously (29). Cardiomyocytes were cultured in DMEM (Sigma-Aldrich) supplemented with 10% FBS (Equitech-Bio). At 6 hours after isolation of cardiomyocytes, cells were transfected with siRNAs (100 nmol/l) using Optifect reagent (Invitrogen) according to the manufacturer's instructions. Both si-cMK (see Supplemental Methods) and si-smMK (see Supplemental Methods) were purchased from B-bridge. As a negative control, cells were transfected with siControl Non-Targeting siRNA#1 (B-bridge). Isolation of mRNA was performed at 24 hours after transfection and protein experiments were performed at 72 hours after transfection. For immunostaining, the same procedures of siRNA transfection were performed in one-fifth scale on Lab-Tek Chamber Slides (nunc).

Cloning of z-cardiac-MLCK. We generated an adult zebrafish cDNA library in Lambda Zap II (Stratagene) using polyA$^+$ RNA from adult zebrafish. The cDNA library was screened with the probe designed to the 5′ side in the ORF of the putative zebrafish ortholog of cardiac-MLCK sequence. Positive phage clone was determined by using phage plaque screen method and single clone excision protocol according to the manufacturer's instructions (Stratagene).

Gene accession numbers. DDBJ accession numbers for the zebrafish MLCK family were as follows: cardiac-MLCK, AB267907; smMLCK, AB267908; skMLCK, AB267909.

Whole-mount in situ hybridization. The digoxigenin-labeled antisense and sense RNA probes (see Supplemental Methods) were transcribed using SP6 and T7 RNA polymerase. Zebrafish embryos at 24 and 48 hpf were fixed with 4% paraformaldehyde, digested with proteinase K, and hybridized with each probe at 68°C. Alkaline-conjugated anti-digoxigenin antibody was used to detect the signals. After staining, embryos were refixed with 4% paraformaldehyde and stored in PBS.

Injection of MO. All MOs were synthesized by Gene-Tools. At cell stages 1–4, 4–10 ng of these MOs were injected into zebrafish embryos. Several data were collected before the 96-hpf stage. Sequences of MOs are available in the Supplemental Methods.

Analysis of zebrafish cardiac histology and cardiac function. We studied hearts of control mock-injected zebrafish embryos and z-cMKaugMO–injected zebrafish embryos at 72 hpf by routine histopathology including transmission electron micrography. To visualize the motion of zebrafish cardiac ventricle, the SAG4A strain of zebrafish, which specifically expresses GFP in its cardiac ventricular wall (14), was applied to MO-mediated gene knockdown experiments. GFP-expressed control mock-injected and z-cMKaugMO–injected zebrafish hearts at 72 hpf were imaged with Leica digital camera DFC 350 FX on a Leica MZ 16 FA fluorescence stereomicroscope. Acquired images were compiled as digital movie files using Leica FW4000 software. Each recorded movie was converted to M-mode image using our original software, and Dd, Ds, FS, and heart rate were measured from the M-mode images.

Experimental protocols of rats. Male Wistar rats (0 days, 1 week, 2 weeks, and 10 weeks for mRNA and protein expression analysis; 8 weeks for production of MI rats; Japan Animals) were used in these experiments. MI was induced by permanent ligation of the left anterior descending coronary artery as previously described (29). The same surgical procedure was performed in a sham-operated group of rats except that the suture around the coronary artery was not tied. Isolation of total RNA was performed at 4 weeks after the onset of MI from noninfarcted myocardiums of resected LVs.

Statistics. Statistical analysis was performed using Mann-Whitney *U* test and single regression analysis. Data are presented as mean ± SEM. A *P* value less than 0.05 was considered significant.

Acknowledgments

We thank Ayako Hara (Core Technology Research Laboratories, Sankyo Co. Ltd.) for 5′-RACE analysis; Junichi Okutsu and Masatoshi Nishimura (Core Technology Research Laboratories, Sankyo Co. Ltd.) for microarray data analysis and critical reading of the manuscript; Tomoko Morita for technical assistance; Yulin Liao, Hidetoshi Okazaki, Hiroyuki Yamamoto, and Hisakazu Kato for thoughtful discussion; and A. Kawahara (Kyoto University) for establishing the zebrafish culture system. This study was supported by a grant from the Japan Cardiovascular Research Foundation; by Grants-in-aid for Human Genome, Tissue Engineering and Food Biotechnology (H13-Genome-011) and for Comprehensive Research on Aging and Health [H13-21 seiki (seikatsu)-23], both Health and Labour Sciences Research Grants from the Ministry of Health, Labor, and Welfare; by the Takeda Science Foundation; and by a Grant-in-aid for Scientific Research (no. 17390229) from the Ministry of Education, Science and Culture of Japan.

Received for publication October 31, 2006, and accepted in revised form June 26, 2007.

Address correspondence to: Seiji Takashima, Department of Cardiovascular Medicine, Health Care Center, Osaka University Graduate School of Medicine, 2-2 Yamadaoka, Suita, Osaka 565-0871, Japan. Phone: 011-816-8679-3472; Fax: 011-816-8679-3473; E-mail: takasima@medone.med.osaka-u.ac.jp.

1. Jessup, M., and Brozena, S. 2003. Heart failure. *N. Engl. J. Med.* **348**:2007–2018.
2. Kamisago, M., et al. 2000. Mutations in sarcomere protein genes as a cause of dilated cardiomyopathy. *N. Engl. J. Med.* **343**:1688–1696.
3. Olson, T.M., Michels, V.V., Thibodeau, S.N., Tai, Y.S., and Keating, M.T. 1998. Actin mutations in dilated cardiomyopathy, a heritable form of heart failure. *Science.* **280**:750–752.
4. Watkins, H., et al. 1995. Mutations in the cardiac myosin binding protein-C gene on chromosome 11 cause familial hypertrophic cardiomyopathy. *Nat. Genet.* **11**:434–437.
5. Collins, J.H. 2006. Myoinformatics report: myosin regulatory light chain paralogs in the human genome. *J. Muscle Res. Cell Motil.* **27**:69–74.
6. Chen, J., et al. 1998. Selective requirement of myosin light chain 2v in embryonic heart function. *J. Biol. Chem.* **273**:1252–1256.
7. Olsson, M.C., Patel, J.R., Fitzsimons, D.P., Walker, J.W., and Moss, R.L. 2004. Basal myosin light chain phosphorylation is a determinant of Ca2+ sensitivity of force and activation dependence of the kinetics of myocardial force development. *Am. J. Physiol. Heart Circ. Physiol.* **287**:H2712–H2718.
8. Kamm, K.E., and Stull, J.T. 2001. Dedicated myosin light chain kinases with diverse cellular functions. *J. Biol. Chem.* **276**:4527–4530.
9. Davis, J.S., et al. 2001. The overall pattern of cardiac contraction depends on a spatial gradient of myosin regulatory light chain phosphorylation. *Cell.* **107**:631–641.
10. Zhi, G., et al. 2005. Myosin light chain kinase and myosin phosphorylation effect frequency-dependent potentiation of skeletal muscle contraction. *Proc. Natl. Acad. Sci. U. S. A.* **102**:17519–17524.
11. Lazar, V., and Garcia, J.G. 1999. A single human myosin light chain kinase gene (MLCK; MYLK). *Genomics.* **57**:256–267.
12. Ruppel, K.M., Uyeda, T.Q., and Spudich, J.A. 1994. Role of highly conserved lysine 130 of myosin motor domain. In vivo and in vitro characterization of site specifically mutated myosin. *J. Biol. Chem.* **269**:18773–18780.
13. Aoki, H., Sadoshima, J., and Izumo, S. 2000. Myosin light chain kinase mediates sarcomere organization during cardiac hypertrophy in vitro. *Nat. Med.* **6**:183–188.
14. Kawakami, K., et al. 2004. A transposon-mediated gene trap approach identifies developmentally regulated genes in zebrafish. *Dev. Cell.* **7**:133–144.
15. Sharma, U.C., Pokharel, S., Evelo, C.T., and Maessen, J.G. 2005. A systematic review of large scale and heterogeneous gene array data in heart failure. *J. Mol. Cell. Cardiol.* **38**:425–432.
16. Herring, B.P., Dixon, S., and Gallagher, P.J. 2000. Smooth muscle myosin light chain kinase expression in cardiac and skeletal muscle. *Am. J. Physiol. Cell Physiol.* **279**:C1656–C1664.
17. Sehnert, A.J., et al. 2002. Cardiac troponin T is essential in sarcomere assembly and cardiac contractility. *Nat. Genet.* **31**:106–110.
18. Bar, H., et al. 2005. Severe muscle disease-causing desmin mutations interfere with in vitro filament assembly at distinct stages. *Proc. Natl. Acad. Sci. U. S. A.* **102**:15099–15104.
19. Ehler, E., Rothen, B.M., Hammerle, S.P., Komiyama, M., and Perriard, J.C. 1999. Myofibrillogenesis in the developing chicken heart: assembly of Z-disk, M-line and the thick filaments. *J. Cell Sci.* **112**:1529–1539.
20. Schonberger, J., et al. 2005. Mutation in the transcriptional coactivator EYA4 causes dilated cardiomyopathy and sensorineural hearing loss. *Nat. Genet.* **37**:418–422.
21. Ebert, A.M., et al. 2005. Calcium extrusion is critical for cardiac morphogenesis and rhythm in embryonic zebrafish hearts. *Proc. Natl. Acad. Sci. U. S. A.* **102**:17705–17710.
22. Davis, J.S., Satorius, C.L., and Epstein, N.D. 2002. Kinetic effects of myosin regulatory light chain phosphorylation on skeletal muscle contraction. *Biophys. J.* **83**:359–370.
23. Dias, F.A., et al. 2006. The effect of myosin regulatory light chain phosphorylation on the frequency-dependent regulation of cardiac function. *J. Mol. Cell. Cardiol.* **41**:330–339.
24. Rottbauer, W., et al. 2006. Cardiac myosin light chain-2: a novel essential component of thick-myofilament assembly and contractility of the heart. *Circ. Res.* **99**:323–331.
25. Schaper, J., et al. 1991. Impairment of the myocardial ultrastructure and changes of the cytoskeleton in dilated cardiomyopathy. *Circulation.* **83**:504–514.
26. Hein, S., Kostin, S., Heling, A., Maeno, Y., and Schaper, J. 2000. The role of the cytoskeleton in heart failure. *Cardiovasc. Res.* **45**:273–278.
27. van der Velden, J., et al. 2003. The effect of myosin light chain 2 dephosphorylation on Ca2+ -sensitivity of force is enhanced in failing human hearts. *Cardiovasc. Res.* **57**:505–514.
28. Margossian, S.S., et al. 1992. Light chain 2 profile and activity of human ventricular myosin during dilated cardiomyopathy. Identification of a causal agent for impaired myocardial function. *Circulation.* **85**:1720–1733.
29. Wakeno, M., et al. 2006. Long-term stimulation of adenosine A2b receptors begun after myocardial infarction prevents cardiac remodeling in rats. *Circulation.* **114**:1923–1932.

Overexpression of Mitochondrial Peroxiredoxin-3 Prevents Left Ventricular Remodeling and Failure After Myocardial Infarction in Mice

Shouji Matsushima, MD; Tomomi Ide, MD, PhD; Mayumi Yamato, PhD; Hidenori Matsusaka, MD; Fumiyuki Hattori, PhD; Masaki Ikeuchi, MD; Toru Kubota, MD, PhD; Kenji Sunagawa, MD, PhD; Yasuhiro Hasegawa, PhD; Tatsuya Kurihara, PhD; Shinzo Oikawa, PhD; Shintaro Kinugawa, MD, PhD; Hiroyuki Tsutsui, MD, PhD

Background—Mitochondrial oxidative stress and damage play major roles in the development and progression of left ventricular (LV) remodeling and failure after myocardial infarction (MI). We hypothesized that overexpression of the mitochondrial antioxidant, peroxiredoxin-3 (Prx-3), could attenuate this deleterious process.

Methods and Results—We created MI in 12- to 16-week-old, male Prx-3–transgenic mice (TG+MI, n=37) and nontransgenic wild-type mice (WT+MI, n=39) by ligating the left coronary artery. Prx-3 protein levels were 1.8 times higher in the hearts from TG than WT mice, with no significant changes in other antioxidant enzymes. At 4 weeks after MI, LV thiobarbituric acid–reactive substances in the mitochondria were significantly lower in TG+MI than in WT+MI mice (mean±SEM, 1.5±0.2 vs 2.2±0.2 nmol/mg protein; n=8 each, $P<0.05$). LV cavity dilatation and dysfunction were attenuated in TG+MI compared with WT+MI mice, with no significant differences in infarct size (56±1% vs 55±1%; n=6 each, P=NS) and aortic pressure between groups. Mean LV end-diastolic pressures and lung weights in TG+MI mice were also larger than those in WT+sham-operated mice but smaller than those in WT+MI mice. Improvement in LV function in TG+MI mice was accompanied by a decrease in myocyte hypertrophy, interstitial fibrosis, and apoptosis in the noninfarcted LV. Mitochondrial DNA copy number and complex enzyme activities were significantly decreased in WT+MI mice, and this decrease was also ameliorated in TG+MI mice.

Conclusions—Overexpression of Prx-3 inhibited LV remodeling and failure after MI. Therapies designed to interfere with mitochondrial oxidative stress including the antioxidant Prx-3 might be beneficial in preventing cardiac failure. **(*Circulation*. 2006;113:1779-1786.)**

Key Words: antioxidants ■ free radicals ■ heart failure ■ myocardial infarction ■ remodeling

Experimental and clinical studies have demonstrated excessive generation of reactive oxygen species (ROS) in failing hearts.[1,2] Among the potential sources of ROS within the heart, mitochondrial electron transport produces superoxide anion ($\cdot O_2^-$) in this disease state.[3] Furthermore, increased ROS leads to mitochondrial DNA (mtDNA) damage and dysfunction.[4,5] Therefore, the intimate link between mitochondrial oxidative stress, mtDNA decline, and mitochondrial dysfunction plays an important role in the development and progression of left ventricular (LV) remodeling and failure that occur after myocardial infarction (MI).

Clinical Perspective p 1786

Peroxiredoxin-3 (Prx-3) is a mitochondrial antioxidant protein and member of the Prx family that can scavenge H_2O_2 in cooperation with thiol and peroxynitrite.[6] In mammals, 6 distinct Prx family members have been identified (Prx-1 through -6). Among the Prxs, Prx-3 is unique because it is localized specifically within the mitochondria.[7] Furthermore, in vivo transfer of the *Prx-3* gene protected neurons against cell death induced by oxidative stress.[8] These beneficial characteristics make Prx-3 an important candidate for therapy against LV failure after MI, in which ROS production has been demonstrated to be increased within the mitochondria.[1-4] Although several previous reports showed the beneficial effects of antioxidants on heart failure,[9,10] no study has ever been performed to specifically examine the protective role of Prx-3. To address these questions, we created transgenic (TG) mice containing the rat *Prx-3* gene. Rat Prx-3–TG mice and their wild-type (WT) littermates were randomized to receive

Received August 10, 2005; revision received January 26, 2006; accepted February 2, 2006.

From the Department of Cardiovascular Medicine, Graduate School of Medical Sciences (S.M., T.I., H.M., M.I., T.K., K.S.), and the Department of Redox Medicinal Science, Graduate School of Pharmaceutical Sciences (M.Y.), Kyushu University, Fukuoka; Biomedical Research Laboratories (F.H., Y.H., T.K., S.O.), Daiichi Suntory Pharma Co, Ltd, Osaka; and the Department of Cardiovascular Medicine (S.K., H.T.), Hokkaido University Graduate School of Medicine, Sapporo, Japan.

Correspondence to Hiroyuki Tsutsui, MD, PhD, Department of Cardiovascular Medicine, Hokkaido University Graduate School of Medicine, Kita-15, Nishi-7, Kita-ku, Sapporo 060-8638, Japan. E-mail htsutsui@med.hokudai.ac.jp

Circulation is available at http://www.circulationaha.org

DOI: 10.1161/CIRCULATIONAHA.105.582239

either a large transmural MI induced by coronary artery ligation or sham operation.

Methods

Generation of TG Mice

The rat Prx-3 cDNA fragment including the entire open reading frame from nucleotide 5 to 802 was amplified by polymerase chain reaction (PCR) and cloned into pCRII (Invitrogen, Carlsbad, Calif). An expression vector for Prx-3 was constructed with pQBI25 (TaKaRa), and the gene for green fluorescent protein was removed at the site of *Nhe*I-*Bam*HI. A cytomegalovirus promoter–driven expression cassette containing rat Prx-3 cDNA in the sense orientation was purified by ultracentrifugation with CsCl. The pronuclei of fertilized eggs from hyperovulated C57BL/6J mice were randomly microinjected with this DNA construct. Tail clips and a PCR protocol to confirm the genotype were performed by one group of investigators. Homozygous TG mice and C57BL/6J WT mice were used at 12 to 16 weeks of age. The study was approved by our institutional animal research committee and conformed to the animal care guidelines of the American Physiological Society.

Creation of MI

We created MI in 12- to 16-week-old, male TG mice (TG+MI) and nontransgenic WT littermates (WT+MI) by ligating the left coronary artery. Sham operation without coronary artery ligation was also performed in WT (WT+sham) and TG (TG+sham) mice. This assignment procedure was performed with the use of numeric codes to identify the animals.

Prx-3 Protein

Prx-3 protein levels were analyzed in cardiac tissue homogenates by Western blot analysis with a monoclonal antibody against rat Prx-3. Our preliminary studies revealed that this antibody against rat Prx-3 cross-reacted with mouse Prx-3 as a single band of 25 kDa. In brief, the LV tissues were homogenized with lysis buffer (20 mmol/L Tris-HCl, 1 mmol/L EDTA, 1 mmol/L EGTA, and 1 mmol/L phenylmethylsulfonylfluoride; pH 7.4). After centrifugation, equal amounts of protein (5 μg protein/lane), estimated by the Bradford method with a protein assay (Bio-Rad, Hercules, Calif), were electrophoresed on a 15% sodium dodecyl sulfate–polyacrylamide gel and then electrophoretically transferred to a nitrocellulose membrane (Millipore, Billerica, Mass). After being blocked with 5% nonfat milk in phosphate-buffered saline (PBS) containing 0.05% Tween 20 at 4°C for 1 hour, the membrane was incubated with the first antibody and then with the peroxidase-linked second antibody (Amersham Pharmacia, Uppsala, Sweden). Chemiluminescence was detected with an enhanced chemiluminescence Western blot detection kit (Amersham Pharmacia) according to the manufacturer's recommendation.

To further assess the subcellular localization of Prx-3 protein, mitochondrial and cytoplasmic fractions were prepared from LVs and subjected to Western blot analysis. In brief, the LV tissues were homogenized at 4°C for 1 minute in 6 volumes of buffer consisting of 10 mmol/L HEPES-NaOH (pH 7.4), 1 mmol/L disodium EDTA, and 250 mmol/L sucrose. The homogenate was centrifuged at 4°C and 3000*g* for 10 minutes to remove any nuclear and myofibrillar debris, and the resultant supernatant was centrifuged at 10 000*g* for 10 minutes to separate any cardiac subcellular fractions. The supernatant was used for the cytoplasmic fraction assay. To isolate the mitochondrial fraction, the pellet was resuspended at 4°C in a buffer consisting of 10 mmol/L HEPES-NaOH (pH 7.4), 1 mmol/L sodium EDTA, and 250 mmol/L sucrose and was washed 3 times with the same buffer. Murine antibodies directed toward glyceraldehyde 3-phosphate dehydrogenase (GAPDH) and cytochrome oxidase (COX) subunit I were also used to verify the integrity of these subcellular fractions.

Immunohistochemistry

Frozen sections of cardiac tissues were incubated in the presence of 100 nmol/L MitoTracker Red CMXRos (Molecular Probes, Eugene, Ore) at 37°C for 20 minutes. We did not repeat the freeze/thaw procedure to avoid the loss of mitochondrial integrity. After being washed with PBS (10 mmol/L sodium phosphate, pH 7.4, and 150 mmol/L NaCl), the sections were fixed with 3.7% formaldehyde for 5 minutes. After being washed, the fixed sections were incubated with 100-fold–diluted anti-rat Prx-3 antibody (10 μg/mL) in PBS at 4°C overnight. Fluorescence images were taken with a confocal laser scanning microscope (Bio-Rad MRC 1024) with laser beams of 488 and 568 nm for excitation.

Myocardial Antioxidant Enzyme Activities and Lipid Peroxidation

For the subsequent biochemical studies, the myocardial tissues with MI were carefully dissected into 3 parts: one consisting of the infarcted LV, one consisting of the border zone LV with the peri-infarct rim (a 1-mm rim of normal-appearing tissue), and one consisting of the remaining noninfarcted (remote) LV. The antioxidant enzymatic activities of superoxide dismutase (SOD), catalase, and glutathione peroxidase (GSHPx) were measured in the noninfarcted LV.[11] The formation of lipid peroxides was measured in the mitochondrial fraction isolated from the LV myocardium with use of a biochemical assay with thiobarbituric acid–reactive substances (TBARS).[4]

Survival

A survival analysis was performed in WT+sham (n=15), TG+sham (n=14), WT+MI (n=39), and TG+MI (n=37) mice. During the study period of 4 weeks, the cages were inspected daily for deceased animals. All deceased mice were examined for the presence of MI as well as pleural effusion and cardiac rupture.

Echocardiographic and Hemodynamic Measurements

At 4 weeks after surgery, echocardiographic studies were performed under light anesthesia with tribromoethanol/amylene hydrate (2.5% wt/vol, 8 μL/g IP) and spontaneous respiration. Two-dimensional, targeted M-mode tracings were recorded at a paper speed of 50 mm/s. Under the same anesthesia with Avertin, a 1.4F micromanometer-tipped catheter (Millar Instruments, Houston, Tex) was inserted into the right carotid artery and then advanced into the LV to measure LV pressures. One subset of investigators who were not informed of the experimental group assignments performed the in vivo LV function studies.

Infarct Size

To measure infarct size 28 days after MI, the heart was excised and the LVs were cut from apex to base into 3 transverse sections. Five-micron sections were cut and stained with Masson's trichrome. Infarct length was measured along the endocardial and epicardial surfaces in each of the cardiac sections, and the values from all specimens were summed. Infarct size (as a percentage) was calculated as total infarct circumference divided by total cardiac circumference.[12]

In addition, to measure infarct size after 24 hours (when most animals were still alive), a separate group of animals including WT+MI (n=5) and TG+MI (n=5) mice was created by ligating the left coronary artery according to the same methods described earlier. After 24 hours of coronary artery ligation, Evans blue dye (1%) was perfused into the aorta and coronary arteries, and tissue sections were weighed and then incubated with a 1.5% triphenyltetrazolium chloride solution. The infarct area (pale), the area at risk (not blue), and the total LV area from each section were measured.[13] In our preliminary study, we confirmed excellent reliability of infarct size measurements, in which a morphometric method similar to that performed in this study was used. The intraobserver and interob-

server variabilities between 2 measurements divided by these means, expressed as a percentage, were each <5%.

Myocardial Histopathology and Apoptosis

Myocyte cross-sectional area and collagen volume fraction were determined by quantitative morphometry of tissue sections from the mid-LV. To detect apoptosis, tissue sections from the mid-LV were stained with terminal deoxynucleotidyl transferase–mediated dUTP nick end-labeling (TUNEL) staining. The number of TUNEL-positive cardiac myocyte nuclei was counted, and the data were normalized per 10^5 total nuclei identified by hematoxylin-positive staining in the same sections. The proportion of apoptotic cells was counted in the noninfarcted LV. We further examined whether apoptosis was present by the more sensitive ligation-mediated PCR fragmentation assays (Maxim Biotech, Inc, Rockville, Md).

mtDNA Copy Number

DNA was extracted from cardiac tissues, and a Southern blot analysis was performed to measure the mtDNA copy number, as described earlier.[4] Primers for the mtDNA probe corresponded to nucleotides 2424 to 3605 of the mouse mitochondrial genome, and those for the nuclear-encoded mouse 18S rRNA probe corresponded to nucleotides 435 to 1951 of the human 18S rRNA genome. The mtDNA levels were normalized to the abundance of the 18S rRNA gene run on the same gel.

Mitochondrial Complex Enzyme Activity

The specific activity of mitochondrial electron transport chain complex I (rotenone-sensitive NADH-ubiquinone oxidoreductase), complex II (succinate-ubiquinone oxidoreductase), complex III (ubiquinol–cytochrome *c* oxidoreductase), and complex IV (cytochrome *c* oxidase) was measured in myocardial tissues according to methods described previously.[4] All enzymatic activities were expressed as nanomoles per minute per milligram protein.

Plasma TBARS

The formation of TBARS in peripheral blood samples from WT+MI and TG+MI mice was measured by a fluorometric assay, as described previously.[14] In brief, 100 μL of whole blood was mixed with 1 mL of saline and centrifuged at 3000*g* for 15 minutes. The supernatant was mixed with 1/12N H_2SO_4 and 10% phosphotungstic acid, and the mixture was centrifuged. The sediment was suspended in distilled water, 0.3% thiobarbituric acid, and 0.1% butylated hydroxytoluene. The reaction mixture was then heated at 100°C for 60 minutes in an oil bath. After being cooled with tap water, the mixture was extracted with *n*-butanol and centrifuged at 1600*g* for 15 minutes. The fluorescence intensity of the organic phase was measured by spectrofluorometry with a wavelength of 510-nm excitation and 550-nm emission. Malondialdehyde standards (Sigma-Aldrich, St. Louis, Mo) were included with each assay batch, and plasma TBARS were expressed as micromoles per gram of plasma protein in reference to these standards.

Statistical Analysis

Data are expressed as mean±SEM. Survival analysis was performed by the Kaplan-Meier method, and between-group differences in survival were tested by the log-rank test. A between-group comparison of means was performed by 1-way ANOVA, followed by *t* tests. The Bonferroni correction was applied for multiple comparisons of means. $P<0.05$ was considered statistically significant.

The authors had full access to the data and take full responsibility for their integrity. All authors have read and agreed to the manuscript as written.

Results

We investigated 4 groups of mice, WT+sham (n=15), TG+sham (n=14), WT+MI (n=39), and TG+MI (n=37), in the present study. A survival analysis was performed for all of these mice. Subsequent echocardiographic and hemodynamic measurements were performed in the 4-week survivors: 15 WT+sham, 14 TG+sham, 25 WT+MI, and 31 TG+MI mice. These measurements could not be accomplished in 4 WT+MI and 5 TG+MI mice owing to technical difficulties. Survivor mice were further divided into 2 groups: those studied for subsequent histological analysis, including infarct size, myocyte size, and collagen volume fraction measurements as well as TUNEL staining (5 WT+sham, 5 TG+sham, 8 WT+MI, and 8 TG+MI), and those for the biochemical assay, including antioxidant enzyme activity, Prx-3 protein levels, mitochondrial lipid peroxidation, mtDNA copy number, and mitochondrial complex enzyme activities (8 WT+sham, 8 TG+sham, 8 WT+MI, and 8 TG+MI). Infarct size was not measured in the mice that died.

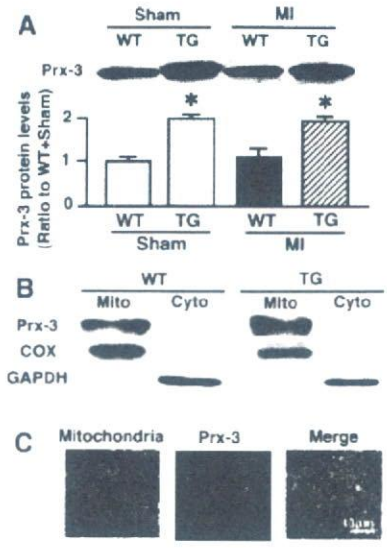

Figure 1. A, Representative Western blot analysis of Prx-3 protein levels (upper panels) and summary data (lower panels) in hearts from WT+sham, TG+sham, WT+MI, and TG+MI mice (n=6 each). Total protein extracts from the hearts were probed with a monoclonal antibody against rat Prx-3. The antibody recognized both rat and mouse Prx-3 as a single band of 25k Da. Data were obtained by densitometric quantification of the Western blots. Values are expressed as the ratio to the WT+sham value and mean±SEM. *$P<0.05$ for the difference from the ratio to WT+sham values. B, Localization of Prx-3 to mitochondria (mito). Western blot analysis of mitochondrial and cytoplasmic (cyto) fractions that were probed with antibodies directed toward Prx-3 as well as specific mitochondrial and cytoplasmic markers: GAPDH was detected in the cytoplasmic but not the mitochondrial fraction, and COX subunit I was detected in the mitochondrial but not the cytoplasmic fraction. Importantly, Prx-3 proteins were detected only in the mitochondrial fraction but not in the cytoplasmic fraction. C, Myocardial tissue sections from TG mice were doubly stained with MitoTracker dye (red) and a rat Prx-3–specific antibody (green). Immunoreactivity for Prx-3 was observed in the cytoplasm of cardiac myocytes. The merged images show that Prx-3 colocalized with the mitochondria (yellow). Scale bar=10 μm.

Myocardial Antioxidants and TBARS

First, baseline differences in Prx-3 proteins as well as other antioxidant enzyme activities between WT and TG mice were determined. In TG+sham, there was a significant increase in Prx-3 protein levels in the LV compared with that of WT+sham (Figure 1A). Importantly, the antioxidants, in-

TABLE 1. Characteristics of Animal Models

	WT+Sham	TG+Sham	WT+MI	TG+MI
Antioxidant enzymes				
n	7	7	7	7
SOD, U/mg protein	26.4±1.1	27.8±1.4	25.1±1.7	23.9±1.2
GSHPx, nmol/min per mg protein	74.1±3.2	77.7±6.7	87.8±4.8	86.1±4.2
Catalase, nmol/mg protein	79.9±6.4	85.0±6.2	87.1±3.5	81.4±5.8
Echocardiographic data				
n	15	14	21	26
Heart rate, bpm	481±11	451±8	463±13	458±8
LVEDD, mm	3.47±0.05	3.37±0.08	5.51±0.13†	4.9±0.10†§
LVESD, mm	2.22±0.05	2.12±0.10	4.78±0.13†	4.08±0.10†§
Fractional shortening, %	35.3±0.8	37.0±1.1	13.1±0.6†	16.9±0.6†§
Hemodynamic data				
n	15	14	21	26
Heart rate, bpm	447±14	455±14	453±9	466±7
Mean aortic pressure, mm Hg	83±3	78±2	76±2	77±3
LVEDP, mm Hg	2.7±0.5	2.5±0.3	11.4±1.5†	7.6±1.0*‡
Organ weight data				
n	15	14	21	26
Body wt, g	26.9±0.5	27.0±0.8	27.0±0.3	26.4±0.4
LV wt/body wt, mg/g	3.2±0.1	3.0±0.1	4.6±0.3†	4.4±0.1†
Lung wt/body wt, mg/g	5.0±0.1	5.2±0.1	7.6±0.5†	6.4±0.3†‡
Pleural effusion, %	0	0	43	15‡

EDD indicates end-diastolic diameter; ESD, end-systolic diameter; and wt, weight. Values are mean±SEM.

*$P<0.05$, †$P<0.01$ vs WT+Sham. ‡$P<0.05$, §$P<0.01$ vs WT+MI.

cluding SOD, GSHPx, and catalase activities, were not altered in the TG hearts (Table 1), indicating no effects of Prx-3 overexpression on other antioxidant enzymes. Second, the changes in antioxidants after MI were assessed. Prx-3 protein levels were significantly higher in TG+MI than in WT+MI (Figure 1A) mice. The activities of other antioxidant enzymes were not altered in WT+MI or TG+MI compared with WT+sham animals (Table 1).

The cytoplasmic marker GAPDH was detected exclusively in the cytoplasmic but not in the mitochondrial fraction, whereas COX subunit I was detected preferentially in the mitochondrial but not in the cytoplasmic fraction. This substantiates the integrity of our cellular fractions. Importantly, Prx-3 was detected only in the mitochondrial fraction but not in the cytoplasmic fraction, further confirming that Prx-3 was localized exclusively in the mitochondria (Figure 1B). In addition, immunohistochemical studies showed a homogeneous Prx-3 distribution in cardiac myocytes that colocalized with the mouse mitochondria (Figure 1C). Prx-3 staining showed a relatively spotty pattern. These results further confirm that the rat Prx-3 transgene is not expressed in the cytoplasm within the mouse heart. Mitochondrial TBARS measured in the noninfarcted LV were significantly greater in WT+MI compared with sham animals and were significantly lower in the TG+MI group (Figure 2).

Survival

There were no deaths in the sham-operated groups. Early operative mortality (within 6 hours) was comparable between WT+MI and TG+MI animals (15% versus 7%; P=NS). The survival rate up to 4 weeks tended to be higher in TG+MI compared with WT+MI mice, but this difference did not reach statistical significance (P=0.06 by log-rank test; Figure 3A). Death was suspected to be attributable to heart failure and/or arrhythmia. Five WT+MI (15%) and 2 TG+MI (5%) mice died of LV rupture (P=NS).

Infarct Size

Infarct size as determined by morphometric analysis 28 days after MI was comparable (55±1% versus 56±1%; P=0.83) between WT+MI (n=6) and TG+MI (n=6) groups. To further confirm that overexpression of Prx-3 did not alter infarct size, both the area at risk and infarct area were

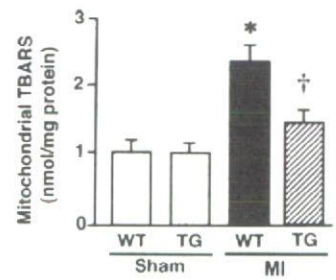

Figure 2. Mitochondrial TBARS in 4 experimental groups of animals (n=8 each). Values are mean±SEM. *$P<0.05$ for difference from the WT+sham value. †$P<0.05$ for difference from the WT+MI value.

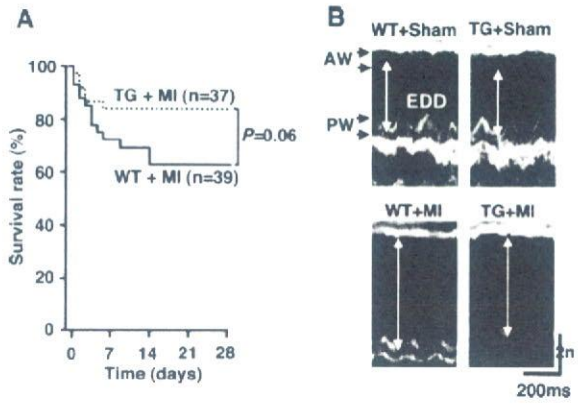

Figure 3. A, Kaplan-Meier survival analysis. Percentages of surviving WT+MI (n=39) and TG+MI (n=37) mice were plotted. Between-group difference was tested by the log-rank test. B, M-mode echocardiograms obtained from WT+sham, TG+sham, WT+MI, and TG+MI mice. AW indicates anterior wall; PW, posterior wall; and EDD, end-diastolic diameter.

measured in mice 24 hours after coronary artery ligation. Percentages of the LV at risk (risk area/LV, 51±3% versus 52±2%; P=0.89) and infarct size (infarct/risk area, 79±1% versus 78±1%; P=0.13) were also comparable between WT+MI (n=5) and TG+MI (n=5) animals.

Echocardiography and Hemodynamics

The echocardiographic and hemodynamic data of surviving mice at 28 days are shown in Figure 3B and Table 1. LV diameters were significantly larger in WT+MI mice with respect to WT+sham animals. TG+MI mice displayed less LV cavity dilatation and greater fractional shortening than did WT+MI mice. There was no significant difference in heart rate or aortic blood pressure among the 4 groups of mice. LV end-diastolic pressure (LVEDP) was higher in WT+MI than in WT+sham animals, but this increase was significantly attenuated in TG+MI mice.

Organ Weights and Histomorphometry

Coincident with an increased LVEDP, lung weight/body weight was larger in WT+MI mice, and this increase was attenuated in TG+MI mice (Table 1). The prevalence of pleural effusion was also lower in TG+MI than in WT+MI groups. Histomorphometric analysis of noninfarcted LV sections showed that myocyte cross-sectional area was greater in WT+MI mice but was significantly attenuated in TG+MI mice (Figure 4). Collagen volume fraction was greater in WT+MI mice, but this change was inhibited in TG+MI mice (Figure 4).

Myocardial Apoptosis

There were rare TUNEL-positive nuclei in sham-operated mice. The number of TUNEL-positive myocytes in the noninfarcted LV was larger in WT+MI mice but was significantly smaller in TG+MI animals (Figure 5A). In addition, the intensity of the DNA ladder indicated that apoptosis in TG+MI animals was decreased compared with that in WT+MI mice (Figure 5B).

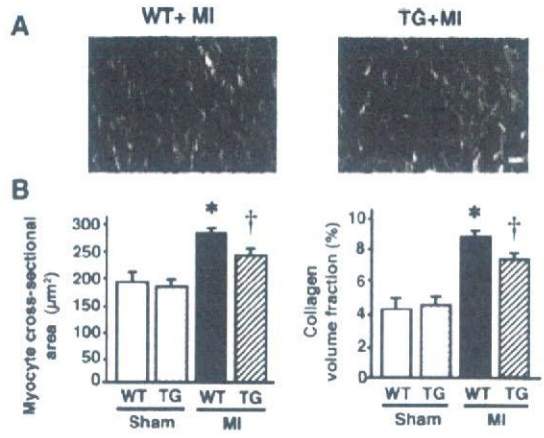

Figure 4. A, Photomicrographs of Masson trichrome–stained LV cross sections obtained from WT+MI and TG+MI mice. Scale bar=10 μm. B, Myocyte cross-sectional area and collagen volume fraction in WT+sham (n=5), TG+sham (n=5), WT+MI (n=8), and TG+MI (n=8) mice. Values are mean±SEM. *P<0.05 for difference from the WT+sham value. †P<0.05 for difference from the WT+MI value.

mtDNA and Mitochondrial Complex Enzymes Activity

Consistent with our previous studies,[4] mtDNA copy number in the noninfarcted LV from WT+MI animals showed a 36% decrease (P<0.05) compared with that in sham-operated mice, which was significantly prevented and was preserved at normal levels in TG+MI animals (Figure 6).

To determine the effects of mtDNA alterations on mitochondrial function, we next measured the mitochondrial electron transport chain complex enzyme activities. The enzymatic activities of complexes I, III, and IV were significantly lower in the noninfarcted LV from WT+MI than in those from WT+sham animals (Table 2). Most important, no such decrease was observed in TG+MI mice. The enzymatic activity of complex II, exclusively encoded by nuclear DNA, was not altered in either group. These results indicate that mtDNA copy number and mitochondrial complex enzymatic activities are downregulated in the post-MI heart and that Prx-3 gene overexpression efficiently counteracts these mitochondrial deficiencies.

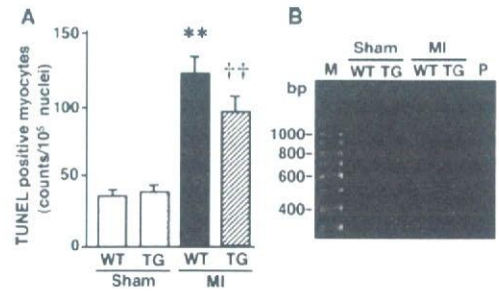

Figure 5. A, Numbers of TUNEL-positive myocytes in the noninfarcted LV from WT+sham, TG+sham, WT+MI, and TG+MI mice (n=5 each). Values are mean±SEM. **P<0.01 for the difference from the WT+sham value. ††P<0.01 for the difference from the WT+MI value. B, DNA ladder indicative of apoptosis in the genomic DNA from the LV. M indicates marker; P, positive control.

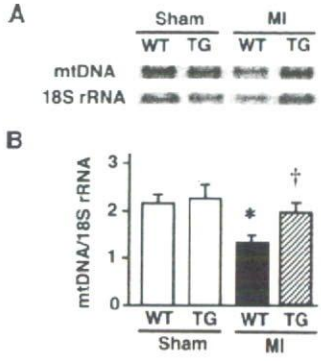

Figure 6. A, Southern blot analysis of mtDNA copy number in total DNA extracts from the hearts from WT+sham, TG+sham, WT+MI, and TG+MI mice. Top bands show signals from the mtDNA fragments, and bottom bands show signals from the nuclear DNA fragments containing the 18S rRNA gene. B, Summary data for a Southern blot analysis of mtDNA copy number in 4 groups of animals (n=8 each). Data were obtained by densitometric quantification of the Southern blots, such as shown in A. Values are expressed as the ratio to WT+sham values and mean±SEM. *$P<0.05$ for the difference from the WT+sham value. †$P<0.05$ for the difference from the WT+MI value.

Plasma TBARS

Plasma TBARS were comparable between WT+MI and TG+MI mice (0.46±0.04 versus 0.54±0.05 μmol/g protein; P=NS).

Discussion

The present study provides the first direct evidence that overexpression of mitochondrial antioxidant Prx-3 protects the heart against post-MI remodeling and failure in mice. It reduced LV cavity dilatation and dysfunction, as well as myocyte hypertrophy, interstitial fibrosis, and apoptosis of the noninfarcted myocardium. These beneficial effects of *Prx-3* gene overexpression were associated with an attenuation of mitochondrial oxidative stress, mtDNA decline, and dysfunction. They were not due to its MI size-sparing effect but occurred secondary to more adaptive remodeling.

Mitochondria are the predominant source of ROS in the failing myocardium.[1] Most of the $\cdot O_2^-$ generated by the mitochondria is vectorially released into the mitochondrial matrix. $\cdot O_2^-$ impairs mitochondrial function by oxidizing the Fe-S centers of complex enzymes. In addition, $\cdot O_2^-$ is converted to peroxynitrite, an extremely powerful oxidant, as a result of its reaction with NO produced by mitochondrial NO synthase. $\cdot O_2^-$ is also converted to H_2O_2 by a specific intramitochondrial Mn-SOD. Although Mn-SOD relieves mitochondrial oxidative stress caused by $\cdot O_2^-$, it generates H_2O_2 and therefore, further enhances a different type of oxidative stress. H_2O_2 can damage cellular macromolecules such as proteins, lipids, and nucleic acids, especially after its conversion to ·OH. Moreover, these increased ROS in the mitochondria were associated with a decreased mtDNA copy number and reduced oxidative capacity owing to low complex enzyme activities.[4] Therefore, chronic increases in mitochondrial ROS production cause mtDNA damage and dysfunction, which thus, can lead to a catastrophic cycle of further oxidative stress and ultimate cellular injury.[5] This deleterious process may play an important role in the development and progression of myocardial remodeling and failure.[4] Based on these results, mitochondrial antioxidants are expected to be the first line-of-defense mechanism against ROS generation in the mitochondria and ROS-mediated mitochondrial injury and thus, may protect the heart from adverse remodeling and failure.

Prx-3, which was formerly known as SP-22, or MER5, is currently identified as a mitochondrial member of the novel antioxidant proteins designated as Prxs.[15] Among 6 known mammalian Prxs, Prx-1 to -4 require the small redox protein thioredoxin (Trx) as an electron donor to remove H_2O_2, whereas Prx-5 and -6 can use other cellular reductants, such as GSH, as their electron donor.[16] Prx-1, -2, and -6 are found in the cytoplasm and nucleus,[7] whereas Prx-3 contains a mitochondrial localization sequence, is found exclusively in the mitochondria, and uses mitochondrial Trx-2 as the electron donor for its peroxidase activity.[17] It functions not only by removing H_2O_2 formed after the SOD-catalyzed dismutation reaction but also by detoxifying peroxynitrite.[6] Therefore, the great efficiency of Prx-3 as an antioxidant shown in the present study may be attributable to the fact that it is located in the mitochondria and can utilize lipid peroxides as well as H_2O_2 for substrates. In fact, overexpression of Prx-3 has been shown to protect thymoma cells from apoptosis induced by hypoxia, a bolus of peroxide, or an anticancer drug.[18] Moreover, Prx-3 overexpression has been reported to protect rat hippocampal neurons from excitotoxic injury.[8] Prx-5 is also associated with the mitochondria in addition to the peroxisomes and nucleus. Recently, increased expression of Prx-5 was found to have protected Chinese hamster ovary cells from mtDNA damage induced by oxidative stress.[19] Therefore, Prx-5 may also exert beneficial effects against mitochondrial oxidative stress in post-MI hearts.

GSHPx also catalyzes the reduction of H_2O_2. In fact, our previous studies demonstrated that overexpression of GSHPx

TABLE 2. Mitochondrial Complex Enzyme Activities

	WT+Sham	TG+Sham	WT+MI	TG+MI
n	7	7	7	7
Complex I, nmol/min per mg protein	282±26	265±38	159±25*	287±16†
Complex II, nmol/min per mg protein	770±70	718±93	711±85	726±128
Complex III, nmol/min per mg protein	505±11	470±31	367±20*	451±21†
Complex IV, nmol/min per mg protein	1223±37	1175±34	744±68*	939±54†

Values are mean±SEM.
*$P<0.05$ vs WT+sham; †$P<0.05$ vs WT+MI.

inhibited LV remodeling and failure after MI.[13] However, GSHPx is located predominantly in the cytosol, and only a small proportion (≈10%) is present in the mitochondria.[20] Therefore, it remains unclear whether the beneficial effects of GSHPx overexpression on post-MI hearts were attributable to an increase of this enzyme in the cytosol, the mitochondria, or both. The specific localization of Prx-3 in the mitochondria suggests that mitochondrial oxidative stress plays an important role in the development and progression of heart failure, and antioxidants localized specifically within the mitochondria provide a primary line of defense against this disease process.

A growing body of evidence suggests that ROS play a major role in the pathogenesis of cardiac failure. Furthermore, antioxidants have been shown to exert protective and beneficial effects against heart failure.[21,22] A previous study from our laboratory demonstrated that dimethylthiourea improved survival and prevented LV remodeling and failure after MI.[10] However, the most effective way to evaluate the contribution of any specific antioxidant and obtain direct evidence of an adverse role for ROS in heart failure is through gene manipulation. Therefore, the present study not only extends the previous observation that used antioxidants but also reveals the major role of mitochondrial oxidative stress in the pathophysiology of post-MI remodeling and failure.

The beneficial effects of Prx-3 overexpression shown in the present study were not due to its MI size-sparing effect, because there was no statistically significant difference in infarct size between WT+MI and TG+MI mice. Furthermore, its effects were not attributable to hemodynamics because blood pressures and heart rates were not altered (Table 1). Importantly, it is also unlikely that these effects were caused by the altered expression of antioxidant enzymes other than Prx-3 (Table 1). Moreover, the beneficial effects of Prx-3 overexpression were not due to systemic induction of antioxidant defenses. This possibility is less likely because plasma TBARS were comparable between WT+MI and TG+MI mice. Nevertheless, we cannot completely exclude the possibility that the systemic effects of Prx-3 induction might also have contributed to this phenotype because this TG is not heart-specific.

There may be several factors contributing to the protective effects conferred by Prx-3 overexpression on post-MI remodeling and failure. First, recent studies have demonstrated that a Trx-related antioxidant system is closely associated with the regulation of apoptosis, probably through quenching of ROS and redox control of the mitochondrial permeability transition pores that release cytochrome *c*.[23] A subtle increase in ROS caused by partial inhibition of SOD results in apoptosis in isolated cardiac myocytes.[24] Previous studies have demonstrated that apoptosis appears not only in infarcted but also in noninfarcted myocardium after MI.[25] Specifically, apoptosis occurs in the noninfarcted LV late after MI. This is an intriguing observation, in light of the remodeling process known to occur within the noninfarcted area, which is characterized by the loss of myocytes and hypertrophy. In fact, recent studies have suggested cardiac myocyte apoptosis contributes to LV remodeling after MI.[26,27] Importantly, increased oxidative stress occurs concomitantly with increased cardiac myocyte apoptosis within the noninfarcted area. This is a provoking observation, because oxidative stress is a powerful inducer of apoptotic cell death.[28] The present study suggests that the coexistence of oxidative stress and myocyte apoptosis in the noninfarcted LV after MI is causally related. Oxidative stress may mediate myocyte apoptosis, which may lead to myocardial remodeling and failure. Therefore, the decreased mitochondrial oxidative stress due to Prx-3 overexpression could contribute to the amelioration of apoptosis (Figure 5) and eventual post-MI cardiac failure. Second, Prx-3 overexpression prevented the decrease in mtDNA copy number (Figure 6) as well as mitochondrial complex enzyme activities (Table 2). Our previous studies have demonstrated an intimate link between mtDNA damage, increased lipid peroxidation, and a decrease in mitochondrial function, which might play a major role in the development and progression of cardiac failure.[4]

There are several issues to be acknowledged as limitations of this study. First, the differences between WT+MI and TG+MI groups in their echocardiographic measurements are not remarkable, even though they are statistically significant (Table 1). However, our previous study showed that the intraobserver and interobserver variabilities in our echocardiographic measurements for LV dimensions were small, and measurements made in the same animals on separate days were highly reproducible.[12] Therefore, these values are considered to be valid. Second, longer-term follow-up data are not available for the animals in the current study. We therefore could not determine whether the differences between WT+MI and TG+MI groups seen in the present study were more or less significant at later time points, when additional LV remodeling would have been expected to occur.

In conclusion, Prx-3 overexpression inhibited the development of LV remodeling and failure after MI, which was associated with an attenuation of myocyte hypertrophy, apoptosis, and interstitial fibrosis. It also ameliorated mitochondrial oxidative stress as well as mtDNA decline and mitochondrial dysfunction in post-MI hearts. Therapies designed to interfere with mitochondrial oxidative stress could be beneficial to prevent heart failure after MI.

Acknowledgments

This study was supported in part by grants from the Ministry of Education, Science and Culture (No. 12670676, 14370230, 17390223). A portion of this study was conducted at Kyushu University Station for Collaborative Research I and II.

Disclosures

None.

References

1. Ide T, Tsutsui H, Kinugawa S, Suematsu N, Hayashidani S, Ichikawa K, Utsumi H, Machida Y, Egashira K, Takeshita A. Direct evidence for increased hydroxyl radicals originating from superoxide in the failing myocardium. *Circ Res*. 2000;86:152–157.
2. Mallat Z, Philip I, Lebret M, Chatel D, Maclouf J, Tedgui A. Elevated levels of 8-iso-prostaglandin F2α in pericardial fluid of patients with heart failure: a potential role for in vivo oxidant stress in ventricular dilatation and progression to heart failure. *Circulation*. 1998;97:1536–1539.

3. Ide T, Tsutsui H, Kinugawa S, Utsumi H, Kang D, Hattori N, Uchida K, Arimura K, Egashira K, Takeshita A. Mitochondrial electron transport complex I is a potential source of oxygen free radicals in the failing myocardium. *Circ Res*. 1999;85:357–363.
4. Ide T, Tsutsui H, Hayashidani S, Kang D, Suematsu N, Nakamura K, Utsumi H, Hamasaki N, Takeshita A. Mitochondrial DNA damage and dysfunction associated with oxidative stress in failing hearts after myocardial infarction. *Circ Res*. 2001;88:529–535.
5. Suematsu N, Tsutsui H, Wen J, Kang D, Ikeuchi M, Ide T, Hayashidani S, Shiomi T, Kubota T, Hamasaki N, Takeshita A. Oxidative stress mediates tumor necrosis factor-α–induced mitochondrial DNA damage and dysfunction in cardiac myocytes. *Circulation*. 2003;107:1418–1423.
6. Bryk R, Griffin P, Nathan C. Peroxynitrite reductase activity of bacterial peroxiredoxins. *Nature*. 2000;407:211–215.
7. Kang SW, Chae HZ, Seo MS, Kim K, Baines IC, Rhee SG. Mammalian peroxiredoxin isoforms can reduce hydrogen peroxide generated in response to growth factors and tumor necrosis factor-α. *J Biol Chem*. 1998;273:6297–6302.
8. Hattori F, Murayama N, Noshita T, Oikawa S. Mitochondrial peroxiredoxin-3 protects hippocampal neurons from excitotoxic injury in vivo. *J Neurochem*. 2003;86:860–868.
9. Sia YT, Lapointe N, Parker TG, Tsoporis JN, Deschepper CF, Calderone A, Pourdjabbar A, Jasmin JF, Sarrazin JF, Liu P, Adam A, Butany J, Rouleau JL. Beneficial effects of long-term use of the antioxidant probucol in heart failure in the rat. *Circulation*. 2002;105:2549–2555.
10. Kinugawa S, Tsutsui H, Hayashidani S, Ide T, Suematsu N, Satoh S, Utsumi H, Takeshita A. Treatment with dimethylthiourea prevents left ventricular remodeling and failure after experimental myocardial infarction in mice: role of oxidative stress. *Circ Res*. 2000;87:392–398.
11. Ho YS, Magnenat JL, Bronson RT, Cao J, Gargano M, Sugawara M, Funk CD. Mice deficient in cellular glutathione peroxidase develop normally and show no increased sensitivity to hyperoxia. *J Biol Chem*. 1997;272:16644–16651.
12. Shiomi T, Tsutsui H, Hayashidani S, Suematsu N, Ikeuchi M, Wen J, Ishibashi M, Kubota T, Egashira K, Takeshita A. Pioglitazone, a peroxisome proliferator–activated receptor-γ agonist, attenuates left ventricular remodeling and failure after experimental myocardial infarction. *Circulation*. 2002;106:3126–3132.
13. Shiomi T, Tsutsui H, Matsusaka H, Murakami K, Hayashidani S, Ikeuchi M, Wen J, Kubota T, Utsumi H, Takeshita A. Overexpression of glutathione peroxidase prevents left ventricular remodeling and failure after myocardial infarction in mice. *Circulation*. 2004;109:544–549.
14. Ide T, Tsutsui H, Ohashi N, Hayashidani S, Suematsu N, Tsuchihashi M, Tamai H, Takeshita A. Greater oxidative stress in healthy young men compared with premenopausal women. *Arterioscler Thromb Vasc Biol*. 2002;22:438–442.
15. Wood ZA, Schroder E, Robin Harris J, Poole LB. Structure, mechanism and regulation of peroxiredoxins. *Trends Biochem Sci*. 2003;28:32–40.
16. Fisher AB, Dodia C, Manevich Y, Chen JW, Feinstein SI. Phospholipid hydroperoxides are substrates for non-selenium glutathione peroxidase. *J Biol Chem*. 1999;274:21326–21334.
17. Watabe S, Hiroi T, Yamamoto Y, Fujioka Y, Hasegawa H, Yago N, Takahashi SY. SP-22 is a thioredoxin-dependent peroxide reductase in mitochondria. *Eur J Biochem*. 1997;249:52–60.
18. Nonn L, Berggren M, Powis G. Increased expression of mitochondrial peroxiredoxin-3 (thioredoxin peroxidase-2) protects cancer cells against hypoxia and drug-induced hydrogen peroxide–dependent apoptosis. *Mol Cancer Res*. 2003;1:682–689.
19. Banmeyer I, Marchand C, Clippe A, Knoops B. Human mitochondrial peroxiredoxin 5 protects from mitochondrial DNA damages induced by hydrogen peroxide. *FEBS Lett*. 2005;579:2327–2333.
20. Chang TS, Cho CS, Park S, Yu S, Kang SW, Rhee SG. Peroxiredoxin III, a mitochondrion-specific peroxidase, regulates apoptotic signaling by mitochondria. *J Biol Chem*. 2004;279:41975–41984.
21. Dhalla AK, Hill MF, Singal PK. Role of oxidative stress in transition of hypertrophy to heart failure. *J Am Coll Cardiol*. 1996;28:506–514.
22. Nakamura R, Egashira K, Machida Y, Hayashidani S, Takeya M, Utsumi H, Tsutsui H, Takeshita A. Probucol attenuates left ventricular dysfunction and remodeling in tachycardia-induced heart failure: roles of oxidative stress and inflammation. *Circulation*. 2002;106:362–367.
23. Petronilli V, Costantini P, Scorrano L, Colonna R, Passamonti S, Bernardi P. The voltage sensor of the mitochondrial permeability transition pore is tuned by the oxidation-reduction state of vicinal thiols: increase of the gating potential by oxidants and its reversal by reducing agents. *J Biol Chem*. 1994;269:16638–16642.
24. Siwik DA, Tzortzis JD, Pimental DR, Chang DL, Pagano PJ, Singh K, Sawyer DB, Colucci WS. Inhibition of copper-zinc superoxide dismutase induces cell growth, hypertrophic phenotype, and apoptosis in neonatal rat cardiac myocytes in vitro. *Circ Res*. 1999;85:147–153.
25. Palojoki E, Saraste A, Eriksson A, Pulkki K, Kallajoki M, Voipio-Pulkki LM, Tikkanen I. Cardiomyocyte apoptosis and ventricular remodeling after myocardial infarction in rats. *Am J Physiol Heart Circ Physiol*. 2001;280:H2726–H2731.
26. Sam F, Sawyer DB, Chang DL, Eberli FR, Ngoy S, Jain M, Amin J, Apstein CS, Colucci WS. Progressive left ventricular remodeling and apoptosis late after myocardial infarction in mouse heart. *Am J Physiol Heart Circ Physiol*. 2000;279:H422–H428.
27. Oskarsson HJ, Coppey L, Weiss RM, Li WG. Antioxidants attenuate myocyte apoptosis in the remote non-infarcted myocardium following large myocardial infarction. *Cardiovasc Res*. 2000;45:679–687.
28. von Harsdorf R, Li PF, Dietz R. Signaling pathways in reactive oxygen species–induced cardiomyocyte apoptosis. *Circulation*. 1999;99:2934–2941.

CLINICAL PERSPECTIVE

A growing body of evidence suggests that oxidative stress, an excess generation of reactive oxygen species (ROS), plays a major role in the pathogenesis of heart failure. Furthermore, antioxidants have been shown to exert protective and beneficial effects against this process. Recent studies have suggested that mitochondria are the predominant source of ROS in the failing heart, and mitochondrial antioxidants are expected to be the first line of defense against mitochondrial oxidative stress–mediated myocardial injury. The present study demonstrated that overexpression of peroxiredoxin-3 (Prx-3) inhibited cardiac remodeling and failure after myocardial infarction (MI) created by ligation of the left coronary artery in mice. Prx-3 contains a mitochondrial localization sequence, is found exclusively in the mitochondria, and uses mitochondrial thioredoxin (Trx)-2 as the electron donor for its peroxidase activity. It functions not only by removing H_2O_2 formed after the superoxide dismutase (SOD)–catalyzed dismutation reaction but also by detoxifying peroxynitrite. Therefore, the great efficiency of Prx-3 as an antioxidant shown in the present study may be attributable to the fact that it is located in the mitochondria and can utilize lipid peroxides as well as H_2O_2 for substrates. The present study not only extends previous investigations that used antioxidants but also reveals a major role for mitochondrial oxidative stress in the pathophysiology of postinfarct heart failure. Therapies designed to interfere with mitochondrial oxidative stress by using antioxidant Prx-3 might also beneficial in preventing clinical heart failure.

Journal of the American College of Cardiology
© 2008 by the American College of Cardiology Foundation
Published by Elsevier Inc.

Vol. 51, No. 24, 2008
ISSN 0735-1097/08/$34.00
doi:10.1016/j.jacc.2007.11.085

Prognostic Utility of B-Type Natriuretic Peptide Assessment in Stable Low-Risk Outpatients With Nonischemic Cardiomyopathy After Decompensated Heart Failure

Mototsugu Nishii, PHD, MD, Takayuki Inomata, PHD, MD, Hitoshi Takehana, PHD, MD, Takashi Naruke, MD, Tomoyoshi Yanagisawa, MD, Masahiko Moriguchi, PHD, MD, Sadao Takeda, PHD, MD, Tohru Izumi, PHD, MD

Sagamihara, Japan

Objectives We investigated the clinical utility of B-type natriuretic peptide (BNP) assay in stable outpatients with nonischemic dilated cardiomyopathy (NICM) after decompensated heart failure (HF).

Background Patients with NICM admitted for decompensated HF frequently experience sudden death or redecompensation after hospital discharge. The prognostic value of BNP during hospitalization has been demonstrated. However, clinical utility of BNP in stable outpatient setting has been poorly investigated.

Methods Eighty-three NICM outpatients who were clinically stable in New York Heart Association functional class 1 to 2 for 6 months after discharge for decompensated HF were enrolled, and then followed for an additional 18 months. The main end point was first readmission for decompensated HF or death. B-type natriuretic peptide levels were measured at 3-month intervals from discharge to enrollment, and echocardiographic dimensions at discharge and enrollment.

Results Mean discharge BNP level was 210 ± 148 pg/ml. Twenty-eight patients were readmitted for decompensated HF or suddenly died at a median time of 11 months from the time of discharge. Among various variables including BNP measurements, clinical parameters and echocardiographic dimensions, a 6-month post-discharge BNP of >190 pg/ml was most closely associated with combined event in the Cox proportional hazards model (hazard ratio 2.29; 95% confidence interval 1.42 to 3.56; p = 0.0005), and had the best discriminatory power (area under the receiver operating characteristic curve 0.91, sensitivity 96%; specificity 76%).

Conclusions Even in stable low-risk outpatients with NICM at 6 months after hospital discharge for decompensated HF, BNP assessment predicts a long-term risk of redecompensation. (J Am Coll Cardiol 2008;51:2329–35) © 2008 by the American College of Cardiology Foundation

Decompensated heart failure (HF) is a critical complication of nonischemic dilated cardiomyopathy (NICM). Outcome in those patients hospitalized for decompensated HF is often poor, and may include readmission for subsequent HF or sudden death (1–3). A simple biomarker as a prognostic predictor, thus, has been sought.

See page 2336

B-type natriuretic peptide (BNP) is secreted from the overloaded left ventricle (LV), and the circulating levels adversely increase in accordance with the degree of LV wall stretch (4,5). Plasma BNP levels have proven utility in many settings, including improving the diagnostic evaluation of acute dyspnea (6,7) as well as the prognostic evaluation of HF patients on both hospital admission and discharge (8–10). However, the clinical utility of BNP assay in stable outpatients after decompensated HF has been poorly investigated. We hypothesized that the prognostic utility of BNP assay would extend to this outpatient setting, albeit with lower cutoff points for high- and low-risk statuses.

Here, we examined the relation of BNP assay with long-term outcome in stable outpatients with NICM after decompensated HF.

From the Department of Cardio-angiology, Kitasato University School of Medicine, Sagamihara, Japan. This study was supported by a Grant-in-Aid for Scientific Research from the Postgraduate Research Project at Kitasato University and a Grant for Scientific Research from the Ministry of Education, Science and Culture of Japan (No. 20311954).

Manuscript received August 22, 2007; revised manuscript received October 18, 2007, accepted November 28, 2007.

JACC Vol. 51, No. 24, 2008
June 17, 2008:2329–35

Abbreviations and Acronyms

ACEI = angiotensin-converting enzyme inhibitor
ARB = angiotensin receptor blocker
BNP = B-type natriuretic peptide
CI = confidence interval
HF = heart failure
HR = hazard ratio
LADd = left atrial diastolic dimension
LV = left ventricle/ventricular
LVDd = left ventricular end-diastolic dimension
LVEF = left ventricular ejection fraction
NICM = nonischemic dilated cardiomyopathy
NYHA = New York Heart Association

Methods

Study population. Informed consent was obtained from all patients for participation in the study in accordance with the protocol, which was approved by the committee on human investigation at our institution. Consecutive outpatients with NICM who were clinically stable in New York Heart Association (NYHA) functional class 1 to 2 for at least 6 months after hospital discharge for decompensated HF were enrolled.

Admission for decompensated HF was determined by adverse cardiac symptoms (NYHA functional class 3 to 4), physical findings (rales and/or S_3 gallop), and evidence of pulmonary congestion or pleural effusion on chest X-ray. Nonischemic dilated cardiomyopathy was diagnosed according to cardiac information during the hospital course including intact coronary arteries on coronary angiography and LV systolic dysfunction (left ventricular ejection fraction [LVEF] of <40%, LV diffuse wall motion abnormality) with a dilated nonhypertrophic LV (left ventricular end-diastolic dimension [LVDd] of >5.5 cm, posterior wall and interventricular septum end-diastolic thickness of ≤1.2 cm) on echocardiography. Echocardiography and cardiac catheterization showed moderate regurgitation of mitral and/or tricuspid valve with the marked dilation of the ventricular cavities in almost all patients, but did not show findings that indicate the existence of primary valvular disease, such as prolapse, structural destruction, extreme calcification, or stenosis.

Discharge criteria were clinically compensated status as follows: NYHA functional class <3, no sign of rales or S3 gallop, stable blood pressure (systolic blood pressure >90 mm Hg), and improvement in renal failure (serum creatinine level <1.5 mg/dl) as well as in chest X-ray findings and HF treatment including beta-blockers, angiotensin-converting enzyme inhibitor (ACEI), and angiotensin receptor blocker (ARB), as recommended by the international guideline (11).

To eliminate the possibility that acute ischemia could precipitate HF decompensation, patients with coronary artery disease were excluded.

Study protocol. Various parameters including BNP level from discharge to enrollment were correlated with outcome. The attending physician was blinded to the BNP results until the end of study.

Outpatient investigations including physical examination, electrocardiogram recording, chest X-ray, and blood sample measurements were conducted every 3 months after discharge. Entry patients were monitored for 18 months after enrollment in the same institutes.

The major end point was sudden death or first readmission for decompensated HF, defined as hospitalization for decompensated HF. The cause of death was determined according to autopsy in all those who died.

Plasma BNP and echocardiographic measurements. Plasma was immediately separated from the blood element by centrifugation at 4°C for the measurement of BNP at discharge, 3 and 6 months after discharge using a specific immunoradiometric assay for human BNP (Shionoria, Osaka, Japan). The minimum detectable quantity of human BNP is 2 pg/ml. The intra-assay and interassay coefficients of variation were 5.2% and 6.1%, respectively.

In accordance with the recommendations of the American Society of Echocardiography, echocardiographic examination was also performed at discharge and 6 months with a Hewlett Packard Sonos 5500 machine (Andover, Massachusetts). Echocardiography was performed by experienced ultrasonographer and repeated by the same operator wherever possible. Left ventricular end-diastolic dimension at the level of the mitral valve leaflet tips and left atrial diastolic dimension (LADd) at the beginning of the QRS complex on the electrocardiography were measured by M-mode echocardiography. Left ventricular ejection fraction was estimated by Simpson's method on 2-dimensional echocardiographs.

Statistical analysis. All values are expressed as mean ± standard deviation. Differences between event-free patients and combined event patients at baseline were tested by using the Student *t* test for continuous variables and the chi-square test with continuity equation for categoric variables. Percentage change in BNP level from discharge to subsequent assay in each patient was expressed as follows: (BNP level at 3 or 6 months − BNP level at discharge) × 100/BNP level at discharge. The predictive values of clinical, echocardiographic, and biochemical variables for combined event of all-cause death and readmission for decompensated HF were examined with a Cox proportional hazards model. To compare the predictive values of the parameters, receiver-operating characteristics and their area under the curve were constructed. The beat prognostic cutoff value for a combined event was defined as that which had the best compromise between sensitivity and specificity for predicting readmission or sudden death. Failure curves were generated by the Kaplan-Meier method, and the log-rank test was used to compare the incidence rate of a combined event or readmission alone among the BNP ranges.

The BNP levels at discharge, 3 and 6 months and echocardiographic parameters at discharge and 6 months in readmitted patients or event-free patients were compared by a multivariate approach to repeated measures using the general linear model, to allow correction for the correlation of repeated observations over time. Probability was significant at the value of $p < 0.05$ level. Statistical analysis was

performed with JMP 6.0 software for Windows (SAS Institute Inc., Cary, North Carolina).

Results

Baseline patient characteristics. None of the 85 consecutive NICM patients discharged with a clinically compensated status was readmitted for decompensated HF within the first 6 months. However, only 2 of those suddenly died of a cardiac event. Finally, the remaining 83 outpatients who were clinically stable for 6 months after hospital discharge were enrolled in this study.

Entry patient characteristics are shown in Table 1. They were from age 25 to 84 years (mean age 56 ± 20 years) and clinically stable in NYHA functional class 1 to 2 at least until enrollment. Mean BNP levels were 210 ± 148 pg/ml at discharge, 182 ± 158 pg/ml at 3 months, and 191 ± 163 pg/ml at 6 months. On echocardiography at discharge, all patients had a dilated LV (mean LVDd 6.4 ± 0.8 cm) and low LV systolic function (mean LVEF 31 ± 8%), while mean LVDd and LVEF at entry of 6.2 ± 1.0 cm and 37 ± 10%, respectively. Other conditions identified in patients included atrial fibrillation (36%), ventricular tachycardia (19%), hypertension (11%), or diabetes (9%). Six patients were implanted with a permanent pacemaker for sick sinus syndrome (n = 2), atrial fibrillation (n = 2), or intraventricular dyssyncrony (n = 2), and an implantable cardioverter-defibrillator was inserted in 2 patients during hospitalization, although 15 patients who had a low LVEF of <36% with nonsustained or sustained ventricular tachycardia were advised of the need for prophylactic implantable cardioverter-defibrillator implantation to reduce the risk of sudden cardiac death (12). No patients required a mechanical circulatory assist device for decompensated congestive HF. Beta-blocker together with ACEI or ARB was initiated, and titrated in a clinically compensated status. However, withdrawal of the beta-blocker was performed in 8 patients early after hospital discharge, because of symptomatic hypotension or marked bradycardia (resting heart rate of <40 beats/min). Among 75 patients with continuous beta-blocker use, mean dosages of carvedilol and metoprolol

Table 1 Baseline Characteristics

	Entire Population (n = 83)	Event-Free (n = 55)	Combined Event (n = 28)	p Value
Age, yrs	56 ± 20	56 ± 12	60 ± 12	0.23
Gender, female, n (%)	24 (29)	14 (25)	10 (34)	0.22
Disease history, n (%)				
Atrial fibrillation	30 (36)	15 (27)	15 (54)	0.018
Ventricular tachycardia	15 (19)	6 (11)	9 (32)	0.017
Hypertension	9 (11)	3 (5)	6 (21)	0.026
Diabetes	7 (9)	5 (10)	2 (7)	0.76
Medication use at enrollment				
Digoxin, n (%)	14 (18)	10 (20)	4 (14)	0.53
Vasodilators, n (%)	7 (9)	5 (10)	2 (7)	0.76
Beta-blocker, n (%)	75 (90)	55 (100)	20 (71)	<0.0001
Carvedilol, mg/day	14 ± 6	16 ± 5	8 ± 5	0.0003
Metoprolol, mg/day	91 ± 40	107 ± 40	64 ± 22	0.036
ACEIs, n (%)	70 (84)	47 (85)	23 (79)	0.69
ARBs, n (%)	16 (20)	10 (20)	6 (21)	0.72
Diuretics, n (%)	27 (33)	14 (25)	13 (38)	0.051
Amiodarone, n (%)	12 (15)	7 (13)	5 (17)	0.53
Permanent pacing, n (%)				
Biventricular pacing	2 (2)	1 (2)	1 (3)	0.62
Cardiac defibrillator	2 (2)	2 (4)	0 (0)	0.31
BNP measurements, pg/ml				
Plasma BNP level at discharge	210 ± 148	188 ± 146	257 ± 148	0.06
Plasma BNP level at 3 months	182 ± 158	141 ± 148	266 ± 154	0.003
Plasma BNP level at 6 months	191 ± 163	108 ± 106	348 ± 142	<0.0001
Echocardiographic parameters				
Left ventricular end-diastolic dimension at discharge, cm	6.4 ± 0.8	6.5 ± 0.8	6.5 ± 0.8	0.41
Left ventricular ejection fraction at discharge, %	31 ± 8	31 ± 9	31 ± 7	0.43
Left atrial diastolic dimension at discharge, cm	4.5 ± 0.9	4.3 ± 0.8	4.8 ± 0.9	0.0061
Left ventricular end-diastolic dimension at enrollment, cm	6.2 ± 1.0	6.0 ± 0.9	6.7 ± 1.0	0.02
Left ventricular ejection fraction at enrollment, %	37 ± 10	39 ± 10	29 ± 9	0.0005
Left atrial diastolic dimension at enrollment, cm	4.5 ± 0.9	4.1 ± 0.8	5.4 ± 0.9	<0.0001
Serum creatinine level at enrollment, mg/dl	1.1 ± 0.2	0.9 ± 0.2	1.2 ± 0.2	0.11

Values are mean ± standard deviation. p values = event-free group versus combined event group.
ACEI = angiotensin-converting enzyme inhibitor; ARB = angiotensin receptor blocker; BNP = B-type natriuretic peptide.

during follow-up were 14 ± 6 mg/day and 91 ± 40 mg/day, respectively. Finally, medical treatment at enrollment consisted of digoxin (18%), vasodilators (9%), beta-blockers (90%), ACEI (84%), ARB (20%), diuretics (33%), and amiodarone (15%).

Outcome. Twenty-three patients were readmitted for decompensated HF, and 5 died suddenly of cardiac events (n = 3) or noncardiac events (n = 2), with a mean or median time from discharge of 11.5 ± 2.9 or 11 months, range 7 to 18 months.

Comparison of clinical characteristics between subgroups. Clinical characteristics are compared between event-free patients and combined event patients in Table 1. Among medications at enrollment, beta-blocker use and dosage of beta-blocker significantly differed between the 2 groups. Among disease history, atrial fibrillation, ventricular tachycardia, and hypertension showed significant differences. Age, gender, and serum creatinine level at enrollment had no significant difference. For BNP measurement, plasma BNP levels at 3 and 6 months showed significant differences between the 2 groups, whereas level at discharge did not. Among echocardiographic parameters, only LVEF and LADd differed.

Cox proportional hazards regression model for predictors of readmission for HF. Associations among BNP measurements as well as clinical and echocardiographic variables for a combined event of death or readmission for decompensated HF were examined using a Cox proportional hazards regression model (Table 2). Among clinical variables, no predictive variables were identified on univariate analysis. For echocardiography, LADd at 6 months was associated with a combined event, notwithstanding the poor predictability of LVEF. For BNP, plasma BNP level at 6 months and percentage change in level between discharge and 6 months were predictive, whereas levels at discharge and 3 months were not. Area under the curve was higher for BNP at 6 months (0.91) than that for the percentage change in BNP between discharge and 6 months (0.83) and LADd at 6 months (0.86).

In multivariate analyses, which were conducted to include significant variables on univariate analysis, only 6-month post-discharge BNP remained a significant predictor of a combined event, with the best cutoff value of 190 pg/ml at this time having 96% sensitivity and 76% specificity (Fig. 1). Six-month post-discharge BNP levels above this cutoff level

Table 2 Univariate and Multivariate Cox Analyses of the Incidence of Death or Readmission for HF

	Analysis for Continuous Variables			Below Vs. Above Median Values			
Variable	HR	95% CI	p Value	Median Level	HR	95% CI	p Value
Univariate analysis							
Age	1.0072	0.9879–1.0264	0.46	56 yrs	1.1895	0.7431–1.9246	0.47
Gender (female)					1.0347	0.5886–2.0433	0.89
Hypertension					1.4902	0.8912–2.2819	0.18
Atrial fibrillation					1.2965	0.8885–2.0973	0.301
Ventricular tachycardia					1.3012	0.9032–2.1693	0.17
Beta-blocker use					1.6691	0.9056–2.5641	0.06
Diuretic use					1.3551	0.8086–2.1936	0.24
Echocardiographic parameters							
Left ventricular end-diastolic dimension at discharge	1.0045	0.7512–1.3283	0.98	6.4 cm	0.8356	0.5189–1.3516	0.48
Left ventricular ejection fraction at discharge	0.9997	0.9715–1.0287	0.99	30%	1.1629	0.7189–1.8729	0.54
Left atrial diastolic dimension at discharge	1.2541	0.9124–1.7142	0.18	4.5 cm	1.3054	0.8106–2.1164	0.28
Left ventricular end-diastolic dimension at 6 months	1.1829	0.9211–1.4969	0.21	6.0 cm	1.3866	0.8383–2.3598	0.22
Left ventricular ejection fraction at 6 months	0.9727	0.9476–0.9978	0.03	36%	1.5019	0.9209–2.4641	0.11
Left atrial diastolic dimension at 6 months	1.8127	1.3143–2.4825	0.0004	4.25 cm	2.0003	1.2436–3.2233	0.0046
BNP measurements							
Plasma BNP level at discharge	1.0008	0.9993–1.0024	0.24	180 pg/ml	1.2642	0.8051–1.9888	0.31
Plasma BNP level at 3 months	1.0013	0.9999–1.0026	0.06	134 pg/ml	1.5097	0.9413–2.4212	0.09
Plasma BNP level at 6 months	1.0043	1.0026–1.0061	<0.0001	174 pg/ml	2.2679	1.4336–3.5863	0.0005
Percentage change in BNP level between discharge and 3 months	1.0002	0.9979–1.0019	0.81	−20.5%	1.4204	0.8863–2.2765	0.14
Percentage change in BNP level between discharge and 6 months	1.0021	1.0000–1.0038	0.049	−11.5%	2.0127	1.2729–3.1757	0.0026
Multivariate analysis							
Plasma BNP level at 6 months	1.0033	1.0011–1.0056	0.0038	174 pg/ml	1.8427	1.1127–3.0426	0.0181
Percentage change in BNP level between discharge and 6 months	1.0016	0.9988–1.0039	0.213	−11.5%	1.6538	0.9991–2.7214	0.051
Left atrial diastolic dimension at 6 months	1.3918	0.9539–2.0027	0.086	4.25 cm	1.5678	0.9486–2.5904	0.0792

BNP = B-type natriuretic peptide; CI = confidence interval; HF = heart failure; HR = hazard ratio

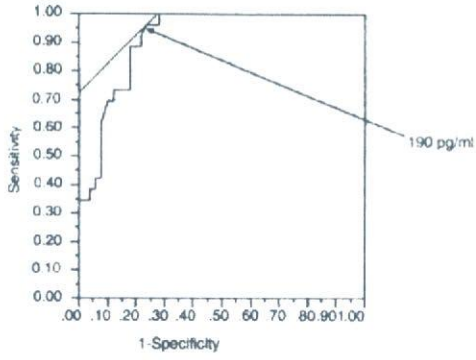

Figure 1 **ROC Curve for Cutoff Values of BNP Levels at 6 Months Post-Discharge**

A B-type natriuretic peptide (BNP) level of 190 pg/ml had the best compromise between sensitivity (96%) and specificity (76%) for predicting readmission for decompensated heart failure or sudden death. ROC = receiver-operating characteristic. Area under curve = 0.91.

strongly related to a combined event (hazard ratio [HR] 2.3; 95% confidence interval [CI] 1.4 to 3.6; p = 0.0005).

Graded relation between 6-month post-discharge BNP level and readmission for HF. Kaplan-Meier curves constructed according to 6-month post-discharge BNP values (Fig. 2A) showed that the risk of a combined event increased in a stepwise fashion across increasing ranges of 6-month post-discharge BNP, namely at <190 pg/ml, 190 to 380 pg/ml, and >380 pg/ml. Patients with a 6-month post-discharge BNP of <190 pg/ml had a better outcome than those at 190 to 380 pg/ml (HR 5.0; 95% CI 2.5 to 9.9) or >380 pg/ml (HR 11.5; 95% CI 4.5 to 29.2). Further, Kaplan-Meier curves for incidence of readmission alone (Fig. 2B) showed the same pattern (HR 4.9 or 13.9; 95% CI 2.5 to 9.8 or 4.5 to 30.1, respectively).

BNP levels and echocardiographic dimensions from discharge to 6 months post-discharge. Event-free patients showed a sustained decrease in BNP level during the 6 months after hospital discharge (mean ± standard error of the mean [SEM] of BNP level, 188 ± 21 pg/ml at discharge, 141 ± 21 pg/ml at 3 months, 108 ± 15 pg/ml at 6 months; discharge vs. 3 months, p = 0.0167; 3 months vs. 6 months, p = 0.0094). In contrast, levels in patients readmitted for decompensated HF did not decrease during follow-up (256 ± 28 pg/ml at discharge, 267 ± 31 pg/ml at 3 months, 349 ± 28 pg/ml at 6 months; discharge vs. 3 months, p = 0.79; 3 months vs. 6 months, p < 0.0001) (Fig. 3A). Regarding changes in echocardiographic dimensions, readmitted patients showed no decrease between discharge and 6 months in LVDd or LADd, or any improvement in LVEF (mean ± SEM at discharge vs. 6 months 6.5 ± 0.1 cm vs. 6.7 ± 0.2 cm, p = 0.07; 4.8 ± 0.2 cm vs. 5.4 ± 0.2 cm, p = 0.0092; 31 ± 1% vs. 29 ± 2%, p = 0.38, respectively), in contrast to event-free patients (6.5 ± 0.1 cm vs. 6.0 ± 0.1 cm, p < 0.0001; 4.3 ± 0.1 cm vs. 4.1 ± 0.1 cm, p = 0.0064; 31 ± 1% vs. 39 ± 1%, p < 0.0001, respectively) (Fig. 3B).

Discussion

Our data show that BNP levels provide important long-term prognostic information even in stable low-risk outpatients after decompensated HF. The increased-risk threshold in healthy population screening is extremely low, on the order of 80 pg/ml as shown in the Framingham data (13). In acute HF or acute coronary syndrome, when BNP levels are elevated, the cutoff point for increased risk increases to about 800 pg/ml as shown by the ADHERE (Acute Decompensated Heart Failure National Registry) data (14). As levels decline over time, however, the cutoff point on the risk assessment curve at hospital discharge falls to about 500 pg/ml (9,10). Our data extend this observation in time, to show a cutoff point of about 200 pg/ml at 6 months after discharge (Fig. 1).

Entry patients in our study represent a low-risk group. They were clinically stable in NYHA functional class 1 to 2 for at least 6 months after discharge for decompensated HF, although Krumholz et al. (1) indicated that almost one-half of all patients admitted for decompensated HF are readmitted within 6 months after discharge. Circulatory stabilization on hospital discharge and socioeconomic status contribute to this favorable clinical course (9,10,15). The 28%

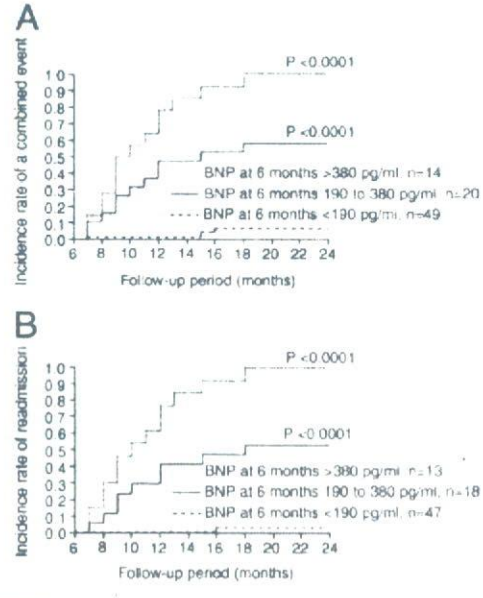

Figure 2 **Kaplan-Meier Analyses**

Kaplan-Meier curves showing the incidence rate of readmission for decompensated heart failure or sudden death **(A)** or of readmission alone **(B)** according to 6-month post-discharge B-type natriuretic peptide (BNP) ranges. B-type natriuretic peptide ranges were <190 (the best cutoff level for predicting readmission or sudden death), 190 to 380, and >380 (its 2-fold level) pg/ml. p < 0.0001 (the log-rank test) versus a BNP range of <190 pg/ml.

JACC Vol. 51, No. 24, 2008
June 17, 2008:2329–35

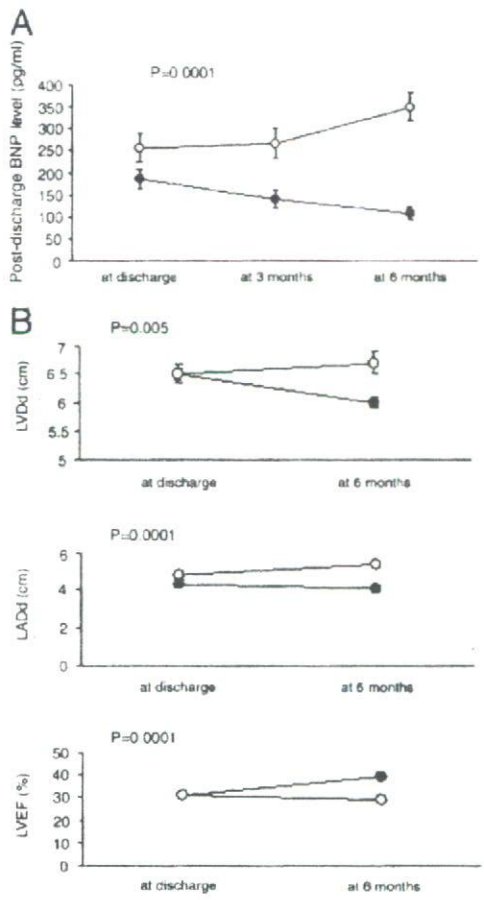

Figure 3 **Changes in BNP Levels and Echocardiographic Findings During a Clinically Compensated Status**

Changes in B-type natriuretic peptide (BNP) at 3-month intervals after hospital discharge **(A)** and in echocardiographic variables between discharge and 6 months **(B)**. **Solid or open circles** indicate BNP levels, echocardiographic dimensions (left ventricular end-diastolic dimension [LVDd]; left atrial diastolic dimension [LADd]), and left ventricular ejection fraction (LVEF) in event-free patients or patients readmitted for decompensated heart failure, respectively. Values are mean ± standard error of the mean. p values comparing changes in BNP and echocardiographic variables between readmitted patients and event-free patients are for repeated measures multivariate analysis of variance over 6 months.

of patients in our study had a discharge BNP level of <100 pg/ml, the optimal level in the exclusion of decompensated HF compared with only 10% in previous study (16), and our population had an extremely low median BNP level of about 200 pg/ml at discharge (Table 1). In addition, our patients received sufficient therapy for decompensated HF without socioeconomic restriction. With regard to the association between female gender and mortality, limited data exist in patients with dilated cardiomyopathy (17), and the very small number of women in our population (Table 1) may also reflect that we selected a low-risk population.

Even this low-risk group had a long-term risk of readmission for decompensated HF or sudden death, despite HF treatment including beta-blocker and ACEI, as recommended by the international guideline (11). This discrepancy can be explained by low maintenance dosages of and withdrawal of beta-blockers (18,19). Dosages of beta-blockers in our population were extremely lower compared with those reached during recent multicenter trials (20,21), and patients who underwent the withdrawal of beta-blockers were readmitted (Table 1). In addition, some patients might be nonresponders to chronic beta-blocker therapy (22). It is also possible that disease history of arrhythmias might also affect outcome (23,24), although we could not confirm its prognostic role (Table 2).

Our data also show that 6-month post-discharge BNP is closely associated with long-term outcome in this observational series, but BNP at 3 months as well as at discharge is not predictive of it (Table 2). In particular, the risk of readmission for decompensated HF adversely increased along with increasing ranges of this level, although we were unable to confirm an association with sudden death, owing to the small number of patients who died (Fig. 2). High plasma levels of BNP have been identified as major predictors of progressive LV remodeling after acute myocardial infarction (25). In our study, readmitted patients, in contrast to event-free patients, showed an increase in BNP levels despite clinical stabilization and had no improvement in echocardiographic parameters during the 6 months follow-up (Fig. 3). Increases in 6-month post-discharge BNP before clinical evidence of decompensation in part reflect a poor reverse LV remodeling. Beta-blockers have been shown to reverse LV remodeling (26) and to improve clinical outcome in patients with HF (20,21). Even in clinically stable low-risk group, higher-risk outpatients with a relatively high level of BNP, thus, may require an optimization of HF treatment including beta-blocker, implying the potential role of BNP as a therapeutic guide even in a stable outpatient setting.

Among several echocardiographic parameters, only LADd at 6 months showed a significant association with outcome (Table 2). The left atrium acts as a reservoir during LV systole (27), and LV diastolic dysfunction results in left atrial overload (28). Enlargement of the LADd may in part reflect adverse LV diastolic dysfunction. However, this variable showed no predictive power in multivariate analysis, including BNP level. But previous reports in patients with HF have described an association between LV diastolic dysfunction and outcome (29,30). Here, the involvement of patients with tachycardia, atrial fibrillation, or permanent pacing meant that we were unable to confirm the predictive power in LV diastolic filling pattern.

Our data offer circumstantial, indirect support for the setting of a target BNP level of <200 pg/ml in the outpatient management of HF, as originally hypothesized by the STARS-BNP (Plasma Brain Natriuretic Peptide-Guided Therapy to Improve Outcome in Heart Failure) multicenter study (31). The number of patients in our study is, however, relatively small, and additional prospective

multicenter studies will be necessary both to confirm our observation and to test a therapeutic utility of BNP assessment in stable HF outpatients.

Conclusions

To our knowledge, this study is the first to indicate that even in low-risk outpatients with nonischemic dilated cardiomyopathy who have been asymptomatic for 6 months after hospital discharge for decompensated HF, BNP assessment identifies a long-term risk of readmission for decompensated HF. Our data confirm and extend the clinical utility of BNP assessment in patients with HF.

Acknowledgment

The authors thank Guy Harris for restyling the manuscript.

Reprints requests and correspondence: Dr. Mototsugu Nishii, Department of Cardio-angiology, Kitasato University School of Medicine, 1-15-1 Kitasato, Sagamihara, 228-8555 Kanagawa, Japan. E-mail: mototsugu555@yahoo.co.jp.

REFERENCES

1. Krumholz HM, Parent EM, Tu N, et al. Readmission after hospitalization for congestive heart failure among Medicare beneficiaries. Arch Intern Med 1997;157:99–104.
2. Haldeman GA, Groft JB, Giles WH, Rashidee A. Hospitalization of patients with heart failure: national hospital discharge survey 1985–1995. Am Heart J 1999;137:352–60.
3. Cowie MR, Fox KF, Wood DA, et al. Hospitalization of patients with heart failure: a population-based study. Eur Heart J 2002;23:877–85.
4. Yoshimura M, Yasue H, Okamura K, Ogawa H, Jougasaki M, Kukoyama M. Different secretion pattern of atrial natriuretic peptide and brain natriuretic peptide in patients with congestive heart failure. Circulation 1993;87:464–9.
5. Yasue H, Yoshimura M, Sumida H, et al. Localization and mechanism of secretion of B-type natriuretic peptide in comparison with those of A-type natriuretic peptide in normal subjects and patients with heart failure. Circulation 1994;90:195–203.
6. Maisel AS, Krishnaswamy P, Nowak RM, et al., Breathing Not Properly Multinational Study Investigators. Rapid measurement of B-type natriuretic peptide in the emergency diagnosis of heart failure. N Engl J Med 2002;347:161–7.
7. Morrison LK, Harrison A, Krishnaswamy P, Kazanegra R, Clopton P, Maisel A. Utility of a rapid B-natriuretic peptide (BNP) assay in differentiating CHF from lung disease in patients presenting with dyspnea. J Am Coll Cardiol 2002;39:202–9.
8. Cheng VL, Kazanegra R, Garcia A, et al. A rapid bedside test for B-type natriuretic peptide predicts treatment outcomes in patients admitted with decompensated heart failure. J Am Coll Cardiol 2001;37:386–91.
9. Logeart D, Thabut G, Jourdain P, et al. Predischarge B-type natriuretic peptide assay for identifying patients at high risk of re-admission after decompensated heart failure. J Am Coll Cardiol 2004;43:635–41.
10. Verdiani V, Nozzoli C, Bacci F, et al. Pre-discharge B-type natriuretic peptide predicts early recurrence of decompensated heart failure in patients admitted to a general medical unit. Eur J Heart Fail 2005;7:566–71.
11. Hunt SA, Baker DW, Chin MH, et al. ACC/AHA guidelines for the evaluation and management of chronic heart failure in the adult: executive summary. A report of the American College of Cardiology/American Heart Association Task Force on Practice Guidelines (Committee to Revise the 1995 Guidelines for the Evaluation and Management of Heart Failure). J Am Coll Cardiol 2001;38:2101–13.
12. Kadish A, Dyer A, Daubert JP, et al., Defibrillators in Non-Ischemic Cardiomyopathy Treatment Evaluation (DEFINITE) Investigators. Prophylactic defibrillator implantation in patients with nonischemic dilated cardiomyopathy. N Engl J Med 2004;350:2151–8.
13. Wang TJ, Larson MG, Levy D, et al. Plasma natriuretic peptide levels and the risk of cardiovascular events and death. N Engl J Med 2004;350:655–63.
14. Fonarow GC, Peacock WF, Phillips CO, Givertz MM, Lopatin M, ADHERE Scientific Advisory Committee and Investigators. Admission B-type natriuretic peptide levels and in-hospital mortality in acute decompensated heart failure. J Am Coll Cardiol 2007;49:1943–50.
15. Rathore SS, Masoudi FA, Wang Y, et al. Socioeconomic status, treatment, and outcomes among elderly patients hospitalized with heart failure: findings from the National Heart Failure Project. Am Heart J 2006;152:371–8.
16. Hogenhuis J, Voors AA, Jaarsma T, Hillege HL, Hoes AW, van Veldhuisen DJ. Low prevalence of B-type natriuretic peptide levels < 100 pg/ml in patients with heart failure at hospital discharge. Am Heart J 2006;151:1012–5.
17. Bourassa MG, Gurne O, Bangdiwala SI, et al. Natural history and patterns of current practice in heart failure. J Am Coll Cardiol 1993;22 Suppl A:14–9.
18. Ruta J, Ptaszynski P, Maciejewski M, Goch JH, Chizynski K. Effect of low doses of metoprolol, bisoprolol and carvedilol on mortality in patients with left ventricular dysfunction after acute myocardial infarction [in Polish]. Wiad Lek 2006;59:649–53.
19. Waagstein F, Caidahl K, Wallentin I, Bergh CH, Hjalmarson A. Long-term beta-blockade in dilated cardiomyopathy. Effects of short- and long-term metoprolol treatment followed by withdrawal and readministration of metoprolol. Circulation 1989;80:551–63.
20. Packer M, Bristow MR, Cohn JN, et al., U.S. Carvedilol Heart Failure Study Group. The effect of carvedilol on morbidity and mortality in patients with chronic heart failure. N Engl J Med 1996;334:1349–55.
21. The MERIT-HF Study Group. Effect of metoprolol CR/XL in chronic heart failure: Metoprolol CR/XL Randomized Intervention Trial in Congestive Heart Failure (MERIT-HF). Lancet 1999;353:2001–7.
22. Di Lenarda A, Sabbadini G, Salvatore L, et al., the Heart-Muscle Disease Study Group. Long-term effects of carvedilol in idiopathic dilated cardiomyopathy with persistent left ventricular dysfunction despite chronic metoprolol. J Am Coll Cardiol 1999;33:1926–34.
23. Wojtkowska I, Sobkowicz B, Musial WJ, Kozuch M. Persistent atrial fibrillation as a prognostic factor of outcome in patients with advanced heart failure [in Polish]. Kardiol Pol 2006;64:777–83.
24. Olshausen K, Schafer A, Mehmel HC, Schwarz F, Senges J, Kubler W. Ventricular arrhythmia in idiopathic dilated cardiomyopathy. Br Heart J 1984;51:195–201.
25. De Lemos JA, McGuire DK, Drazner MH. B-type natriuretic peptide in cardiovascular disease. Lancet 2003;362:316–22.
26. Doughty RN, Whalley GA, Gamble G, MacMahon S, Sharpe N, on behalf of the Australia-New Zealand Heart Failure Research Collaborative Group. Left ventricular remodeling with carvedilol in patients with congestive heart failure due to ischemic heart disease. J Am Coll Cardiol 1997;29:1060–6.
27. Hoit BD, Shao Y, Gabel M, Walsh RA. In vivo assessment of left atrial contractile performance in normal and pathological conditions using a time-varying elastance model. Circulation 1994;89:1829–38.
28. Dernellis JM, Stefanadis CI, Zacharoulis AA, Toutouzas PK. Left atrial mechanical adaptation to long-standing hemodynamic loads based on pressure-volume relations. Am J Cardiol 1998;81:1138–43.
29. Weener GS, Schaefer C, Dirks R, Figulla HC, Kreuzer H. Prognostic value of Doppler echocardiographic assessment of left ventricular filling in idiopathic dilated cardiomyopathy. Am J Cardiol 1994;73:792–8.
30. Giannuzzi P, Temporelli PL, Bosimini E, et al. Independent and incremental prognostic value of Doppler derived mitral deceleration time of early filling in both symptomatic and asymptomatic patients with left ventricular dysfunction. J Am Coll Cardiol 1996;28:383–90.
31. Jourdain P, Jondeau G, Funck F, et al. Plasma brain natriuretic peptide-guided therapy to improve outcome in heart failure: the STARS-BNP multicenter study. J Am Coll Cardiol 2007;49:1733–9.

Journal of Clinical Pharmacy and Therapeutics (2006) **31**, 535–540

ORIGINAL ARTICLE

Carvedilol accelerate elevation of serum potassium in chronic heart failure patients administered spironolactone plus furosemide and either enalapril maleate or candesartan cilexetil

M. Saito* BS, D. Nakayama† BS, M. Takada‡ PhD, K. Hirooka§ MD PhD and Y. Yasumura§ MD

**Department of Pharmacy, National Hospital Organization Osaka Medical Center, Chuo-ku, Osaka, Japan, †Faculty of Pharmaceutical Sciences, Setsunan University, Hirakata, Osaka, Japan, ‡Division of Practical Pharmacy School of Pharmaceutical Sciences, Kinki University, Higashiosaka, Osaka, Japan and §Department of Cardiovascular Internal Medicine, National Hospital Organization Osaka Medical Center, Chuo-ku, Osaka, Japan*

SUMMARY

Objective: **To retrospectively investigate the effect of carvedilol and spironolactone plus furosemide, administered concomitantly with an angiotensin II converting enzyme inhibitor (ACE-I) or an angiotensin II receptor blocker (ARB) to patients with chronic heart failure (CHF).**
Methods: **Patients with CHF, who visited Departments of Cardiovascular Internal Medicine at the National Hospital Organization Osaka Medical Center, were enrolled for this study. Serum potassium, blood urea nitrogen (BUN), serum creatinine (Scr) and serum sodium were measured in every patient at the time of start of treatment and after 3 and 12 months of treatment. Data from patients in groups A (20 mg/day carvedilol + 25 mg/day spironolactone + 40 mg/day furosemide + an ACE-I) and B (20 mg/day carvedilol + 25 mg/day spironolactone + 40 mg/day furosemide + ARB) were compared.**
Results: **When 20 mg/day carvedilol plus 25 mg/day spironolactone plus 5 mg/day enalapril maleate (enalapril, group A) or 8 mg/day candesartan cilexetil (candesartan, group B) plus 40 mg/day furosemide were used concomitantly, the mean serum potassium increased significantly in both groups of patients. Seven of 59 (11·9%) patients had hyperkalemia (>5·5 mEq/L) during 12 months of treatment whereas 8·5% of patients (five of 59) had hypokalemia (≤3·5 mEq/L).**
Conclusion: **When carvedilol is used concomitantly with spironolactone, furosemide and enalapril or candesartan, it is necessary to monitor serum potassium concentration, even if spironolactone is administered at a low dose of 25 mg/day.**

Keywords: **candesartan cilexetil, carvedilol, enalapril maleate, furosemide, hyperkalemia, spironolactone**

Received 6 March 2006, Accepted 18 July 2006
Correspondence: Makoto Saito, Department of Pharmacy, National Hospital Organization Osaka Medical Center, 2-1-14, Hoenzaka, Chuo-ku, Osaka-City, Osaka 540-0006, Japan. Tel.: +81 6 6942 1331; fax: +81 6 6943 6467; e-mail: m-saito@onh.go.jp

INTRODUCTION

In our previous study, we reported that the occurrence of hyperkalemia in chronic heart failure (CHF) patients administered spironolactone depended on the dose. However, when it is given concomitantly with an angiotensin II converting enzyme inhibitor (ACE-I) or angiotensin II receptor blocker (ARB), the occurrence of hyperkalemia exceeding 5·5 mEq/L may increase even with a spironolactone dose as low as 25 mg/day. In the treatment of CHF patients, the carvedilol prospective randomized cumulative survival (COPERNICUS) trial showed that carvedilol, a non-selective beta-adrenergic blocker, was effective (1). The therapeutic effect of spironolactone for this indication has also been shown in the